Comprehensive Summaries of Uppsala Dissertations
from the Faculty of Medicine 942

Development of *In Vitro* and *Ex Vivo* Positron-Emitting Tracer Techniques and Their Application to Neurotrauma

BY

SVEN SIHVER

ACTA UNIVERSITATIS UPSALIENSIS
UPPSALA 2000

Dissertation for the Degree of Doctor of Medical Science in Pharmacology presented at Uppsala University in 2000

ABSTRACT

Sihver, S. 2000. Development of *in vitro* and *ex vivo* positron-emitting tracer techniques and their application to neurotrauma. Acta Universitatis Upsaliensis. *Comprehensive Summaries of Uppsala Dissertations from the Faculty of Medicine* 942. 52 pp. Uppsala. ISBN 91-554-4771-6.

The use of positron-emitting tracers has been extended beyond tomographic facilities in the last few years, giving rise to a general positron-emitting tracing technique. The methodological part of the present thesis involved the evaluation of the performance of storage phosphor (SP) plates, with tracers labeled with high-energy, short-lived, positron-emitting radionuclides, using homogenized tissue specimens and autoradiography with frozen brain sections. The SP plates showed superior sensitivity and a linear response over a wide radioactivity range. Autoradioradiography provided reliable results due to (a) adequate sensitivity for low radioactivity concentration, (b) an excellent linear range, and (c) satisfactory resolution. Though equilibration time of receptor-ligand interaction was dependent upon section thickness, quantification was possible with thinner sections.

An initial finding using frozen section autoradiography of rat brain and spinal cord showed preferential binding of [^{11}C]4-NMPB, a muscarinic acetylcholine (mACh) receptor antagonist, to the M4 subtype of mACh receptors. Further work to ascertain this specificity, by use of binding studies on cell membranes from CHO-K1 cells expressing individual subtypes of human mACh receptors, suggested lack of subtype selectivity. With respect to the possible clinical use in glutamatergic neuropathology, [^{11}C]cyano-dizocilpine, as a potential PET tracer for the N-methyl-D-aspartate (NMDA) subtype of glutamate receptors, was studied. The *in vivo* visualization of specific binding could not be achieved, though *in vitro* binding demonstrated good specificity and preferential binding to the activated form of the NMDA receptors.

The use of the glucose analogue [^{18}F]fluorodeoxyglucose (FDG) to study glucose utilization was evaluated in experimental traumatic brain injury (TBI). A trauma-induced increased uptake of FDG was seen, whereas the uptake of [1-^{14}C]glucose remained unchanged. This discrepancy might be due to the increased postraumatic affinity of FDG for the endothelial glucose transporter proteins and/or to the hexokinase enzyme. [^{11}C]Cyano-dizocilpine, [^{11}C]4-NMPB, and [^{11}C]flumazenil were utilized in autoradiography to evaluate changes in NMDA, mACh, and $GABA_A$ receptors, respectively, in experimental TBI. Observations showed a global decrease in the binding potential (BP) of (i) [^{11}C]cyano-dizocilpine acutely and 12 hrs after TBI, and (ii) of [^{11}C]4-NMPB at 12 hrs after TBI, and (iii) a decrease in the BP of [^{11}C]flumazenil in the cortex and hippocampus ipsilateral to the site of injury. The demonstrated changes in receptor binding after TBI are indicative of a widely dissipated effect of TBI on the particular neurotransmitter receptor systems as compared with what would be expected from FDG studies after TBI, i.e., a local disturbed neurotransmission.

Key words: Short-lived radionuclides, *in vitro* receptor binding, *in vitro* and *ex vivo* autoradiography, positron emission tomography, benzodiazepine, muscarinic acetylcholine, and NMDA receptors in CNS, experimental neurotrauma.

Sven Sihver, Department of Neuroscience, Unit of Pharmacology, Uppsala University, Box 593, SE-751 24 Uppsala, Sweden

ISSN 0282-7476
ISBN 91-554-4771-6

Printed in Sweden by University Printers, Uppsala 2000

PAPERS DISCUSSED

This thesis is based on the following papers, which will be referred to in the text by their Roman numerals:

I. Sihver W, Sihver S, Bergström M, Murata T, Matsumura K, Onoe H, Andersson Y, Bjurling P, Fasth KJ, Westerberg G, Ögren M, Jacobson G, Lundqvist H, Oreland L, Watanabe Y and Långström B (1997) Methodological aspects for *in vitro* characterization of receptor binding using ^{11}C-labeled receptor ligands: a detailed study with the benzodiazepine receptor antagonist [^{11}C]Ro 15-1788. **Nucl Med Biol 24:723-731**.

II. Sihver S, Sihver W, Bergström M, Höglund AU, Sjöberg P, Långström B and Watanabe Y (1999) Quantitative autoradiography with short-lived PET tracers: a study on muscarinic acetylcholine receptors with N-[^{11}C]methyl-4-piperidylbenzilate. **J Pharm Exp Ther 290:917-922**.

III. Sihver S, Sihver W, Andersson Y, Murata T, Bergström M, Onoe H, Matsumura K, Tsukada H, Oreland L, Långström B and Watanabe Y (1998) *In vitro* and *in vivo* characterization of (+)-3-[^{11}C]cyano-dizocilpine. **J Neural Transm 105:117-131.**

IV. Sihver S, Höglund AU, Abelson K, Långström B, Watanabe Y, Tsukada H, Takahashi K, Suhara T, Bergström M *In vitro* binding of [^{11}C](+)3- and [^{11}C]4-N-methylpiperidylbenzilate to five cloned human muscarinic receptors. **Submitted**.

V. Sihver S, Marklund N, Hillered L, Långström B, Watanabe Y, Bergström M. Comparison of cerebral uptake of [^{18}F]fluorodeoxyglucose, [1-^{14}C]glucose, and [^{99m}Tc]HMPAO, in rats after fluid-percussion brain injury. **Manuscript**.

VI. Sihver S, Marklund N, Hillered L, Långström B, Watanabe Y, Bergström M. Changes in mACh, NMDA and $GABA_A$ receptor binding after lateral fluid-percussion injury: *in vitro* autoradiography of rat brain frozen sections. **Submitted**.

sven_sihver@hotmail.com

CONTENTS

ABBREVIATIONS AND SYMBOLS 5

1. INTRODUCTION 7
Positron-emitting tracers 7
Detection of positrons 7
Detection of γ-rays 8
Positron emission tomography (PET) 8
Receptor binding in general 8
Tracers and their targets in the present work 9
Traumatic brain injury 13
The brain trauma model and glucose metabolism 14
PET in traumatic brain injury 15
Glutamate-, ACh-, and GABAergic neurotransmission in brain trauma 16

2. AIMS OF THE THESIS 17

3. MATERIALS AND METHODS 18
Radiation detection systems (used in all papers) 18
Radiotracers and other chemicals (in all papers) 18
Animals (in all papers) 19
Homogenates of transfected cells (IV) 19
Receptor binding in homogenates (I, III, IV) 19
Frozen-section autoradiography (in all papers excl. I) 20
In vivo PET (in paper III) 22
Parasagittal fluid-percussion brain injury (in paper V,VI) 22
Double-tracer studies (in paper V) 23
Data handling 23

4. RESULTS AND DISCUSSION 23
Establishing *in vitro* receptor binding with PET tracers 23
Receptor binding in homogenates 25
Receptor binding autoradiography, qualitative vs. quantitative 27
Subtype specificity of [^{11}C]4-NMPB 28
[^{11}C]cyano-dizocilpine, tracer only for *in vitro* use? 30
Applying *in vitro* tracer studies in neurotrauma 32
Glucose vs. fluorodeoxyglucose 32
NMDA -, mACh -, and $GABA_A$ receptors after traumatic brain injury 36

5. SUMMARY 40

6. ACKNOWLEDGEMENTS 41

REFERENCES 42

APPENDIX ..... Papers I to VI

ABBREVIATIONS AND SYMBOLS

ANOVA	analysis of variance
BBB	blood-brain barrier
B_{max}	total number of receptors
BP	binding potential
CHO	chinese hamster ovary (- cells)
CNS	central nervous system
DG	2-deoxy-D-glucose
FDG	2-[^{18}F]fluoro-2-deoxy-D-glucose
FPI	fluid-percussion (brain) injury
FWHM	full width of half maximum
$GABA_A$	gamma-aminobutyric acid A (- receptors)
HMPAO	hexamethylpropylene amine oxime
IC_{50}	concentration of unlabeled drug that blocks 50% of the binding of the tracer
K_D	equilibrium dissociation constant
K_i	equilibrium dissociation constant for binding of the unlabeled drug
K_{obs}	observed rate constant
K_{off}	dissociation rate constant
K_{on}	association rate constant
LC	lumped constant
LCMRG	local cerebral metabolic rate of glucose
$M_1 – M_5$	pharmacologically identified mACh receptor subtypes
m1 – m5	molecularly identified mACh receptor subtypes
mACh -	muscarinic acetylcholine (- receptors)
NMDA	N-methyl-D-aspartic acid
4-NMPB	N-methyl-4-piperidyl benzilate
(+)3-NMPB	(+)N-methyl-3-piperidyl benzilate
NMS	N-methyl scopolamine
$P_{(2)}$	(second) pellet (after centrifugation)
PBS	phosphate-buffered saline
PET	positron emission tomography
rCBF	regional cerebral blood flow
ROI	region of interest
SD	standard deviation
SEM	standard error of the mean
SP	storage phosphor
SUV	standardized uptake value
$t_{½ass}$	half-life for association
$t_{½diss}$	half-life for dissociation
TBI	traumatic brain injury

1. INTRODUCTION

1.1 Positron-emitting tracers

In the past few years, the use of positron-emitting tracers has been extended beyond tomographic facilities. They are now used on a regular basis in laboratory experiments to explore ligand-receptor interactions in tissue homogenates,[I,III,IV,228,227] in frozen section autoradiography[II,III,V,VI,80,13,119] and in viable tissue section autoradiography.[178,179,196,267,181,180,182] Careful *in vitro* validation of properties of the candidate ligand increases the chances for its successful application[14] in *in vivo* experiments in larger research animals or in humans. Therefore, PET can also be an acronym for Positron-Emitting Tracing – a general radiotracer technique using positron emitters both *in vivo* and *in vitro*, utilizing their dualistic decay properties. The positron (β^+) is a particle with a positive charge, that eventually interacts with an electron leading to the annihilation and the emission of two high-energy (511 keV) gamma rays at precisely 180º from one another. The positron originates from an extra proton that is incorporated into the nuclei of nitrogen, oxygen, carbon or fluorine, and which thereafter become unstable isotopes. In order to regain the stability and balance between protons and neutrons, the proton is cleared into a positron and a neutron, with the neutron remaining within the nucleus. Incorporation of the extra proton is made in a cyclotron, where a target element is bombarded with accelerated protons or deutrons.

An example is shown in the simplified **diagram 1.1**. For the generation of carbon-11 (^{11}C), the target element is nitrogen gas. Irradiation of nitrogen with high-energy protons results in the generation of ^{11}C and helium. The decay of ^{11}C occurs via emission of a positron, leaving a boron atom (**diagram 1.2**):

$$^{14}_{7}N + p \rightarrow {}^{11}_{6}C + {}^{4}_{2}He \qquad 1.1$$

$$^{11}_{6}C \rightarrow {}^{11}_{5}B + \beta^+ + \text{energy} \qquad 1.2$$

Detection of positrons

Storage phosphor (SP) imaging plates are used for capturing the energy from high-energy beta particles for visualizing and quantifying radioactivity patterns. **Figure 1-1 A** illustrates an SP plate wrapped in a plastic foil. The wrapping is essential in order to avoid contamination and damage by liquid from the sample. The samples are pressed tightly against the SP plates by use of an exposure cassette. Storage phosphors capture nearly every beta particle that reaches the plates, thus making the phospor plate a highly

Panel 1-1: The advantages of storage phosphor technology over film autoradiography.*

- Rapid and simple sample exposure
- Better sensitivity and greater dynamic range
- Lower cost per image
- More accurate quantification
- Isotope versatility (e.g.^{14}C, ^{3}H, ^{125}I, ^{131}I, ^{32}P, ^{33}P, ^{35}S)
- Linear response
- Ready to analyse publication-quality digital images
- Ideal for large user groups and shared facilities

***** more information at: http://www.mdyn.com/products/

sensitive tool. **Figure 1-1, B** demonstrates that the dissipated energy excites electrons to a higher energy state at which they remain until deexcited by laser photons.The laser beam releases the stored image as blue luminescent light, which is collected and stored in digital form. In **Figure 1-1, C,** the screen is prepared for reuse by exposing it to erasing light that erases any remaining residual latent image and background due to natural radiation. In **Panel 1-1,** the advantages of phosphor plates over traditional X-ray films are listed. The SP plates are reusable, and if handled with care, can be used indefinitely.

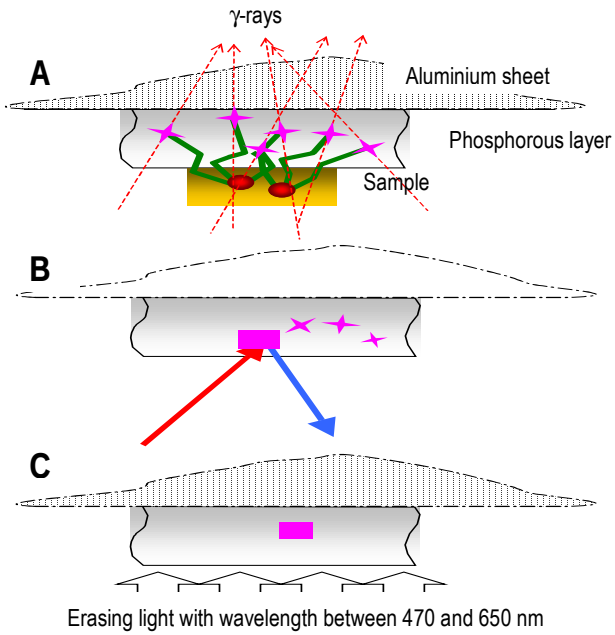

Figure 1-1. Schematic presentation of storage phosphor imaging plates and their use.

Detection of γ-rays

The γ-counter used in this work was a well-type scintillation counter made from tallium-activated sodium iodide (NaI) crystals, which absorb γ-rays efficiently. Light photons that originate in the crystal are detected by a photomultiplicator and recorded. Detectors are shielded from background radiation with 6-cm-thick lead.

Positron emission tomography (PET)

Positron emission tomography (PET) provides a technology where multiple rings of gamma ray detectors are lined around the body. They enable recording of the distribution of an injected or inhaled radioisotope in the tissues (**Figure 1-2**). The two gamma rays emitted by the annihilation of a positron and electron ultimately reach a pair of detectors in a tomograph ring. An event is recorded only when two simultaneous detections are made. That enables localization of a line of gamma emission. After the acquisition of multiples of such emission lines, an image reconstruction program generates images that depict the spatial distribution of radioactivity with a resolution of about 5 mm.

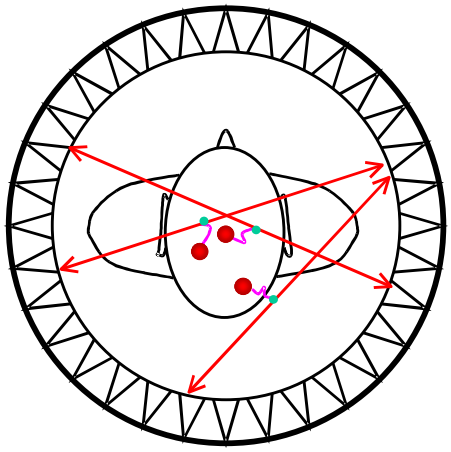

Figure 1-2. In positron emission tomography the γ-rays are detected by an array of crystal photomultipliers that surround the radioactive subject.

1.2 Receptor binding in general.

Receptor binding as used in the *in vitro* investigation of receptors (R) is mostly analyzed according to a bimolecular reaction model (**Diagram 1.3**):

$$L + R \leftrightarrow L{\bullet}R \qquad 1.3$$

Assuming that all receptors are equally accessible to ligand (L), the binding occurs when L and R collide. The number of binding events per unit of time (rate of association) equals $[L]{\bullet}[R]{\bullet}K_{on}$, where K_{on} is the association rate constant (on-rate). Once binding has occurred, the L and R will remain bound together for a random amount of time. The rate of dissociation (off-rate) equals $[L{\bullet}R]{\bullet}K_{off}$, where K_{off} is the dissociation rate constant. At equilibrium, ligand-receptor complexes form at the same rate that they dissociate:

$$[L]{\bullet}[R]{\bullet}K_{on} = [L{\bullet}R]{\bullet}K_{off} \qquad 1.4$$

The **equation 1.4** has been rearranged to define the equilibrium dissociation constant (K_D):

$$K_D = \frac{[L]{\bullet}[R]}{[L{\bullet}R]} = \frac{K_{off}}{K_{on}} \qquad 1.5$$

The concentration of the (radio)ligand-receptor complex [L·R] is frequently referred to as the amount bound [B]. If binding follows the law of mass action (**equation 1.3**), the K_D calculated in **equation 1.5** should be the same as the K_D calculated from a saturation binding curve. For calculating the K_D from saturation binding curve, the non-linear regression is usually transformed to a linear regression by plotting the amount bound on the X axis and the ratio of bound to concentration of free radioligand on the Y axis. The negative reciprocal of the slope of such a plot (Scatchard or Rosenthal plot) is K_D, and the X intercept is the total receptor number (B_{max}).

1.3 Tracers and their targets in the present work.

In PET the following radionuclides ^{15}O, ^{13}N, ^{11}C and ^{18}F with half-lives of 2, 10, 20, and 110 min, respectively, are most interesting.[151] They are produced by nuclear reactions in a cyclotron. The tracers used in the present work are grouped in **Panel 1-2**.

Panel 1-2: Tracers used in this thesis and their targets

Receptor ligands

- [^{11}C]flumazenil → benzodiazepine receptors (I, VI)
- [^{11}C](+)3- and [^{11}C]4-NMPB → mACh receptors (II, IV, VI)
- [^{11}C]cyano-dizocilpine → NMDA receptors (III, VI)

Cerebral blood flow markers

- $C^{15}O_2$ → used *in vivo* (III)
- [^{99m}Tc]HMPAO → used *ex vivo* (V)

Tracers for glucose utilization

- [^{18}F]2-deoxy-D-glucose (V)
- D-[1-^{14}C]glucose (V)

[^{11}C]flumazenil and GABA$_A$ receptor complex. Flumazenil (previously Ro 15-1788) is a selective benzodiazepine receptor antagonist[185,184,73] that binds rapidly and reversibly to its receptors, and shows saturation, and has a low fraction of non-specific binding.[212] The benzodiazepine receptor is a part of the γ-amino butyric acid A ($GABA_A$) receptor-Cl^- channel complex. GABA is a major inhibitory neurotransmitter in the central nervous system (CNS). The substances used for displacement of ^{11}C-flumazenil in the first paper, zolpidem, triazolam and diazepam, are agonistic modulators at the benzodiazepine site and enhance the effects of GABA. Benzodiazepine receptors have been characterized *in*

vitro by use of ^{3}H-labeled ligands, and their regional distribution in the brain and their pharmacological properties have been well described.[238,82,18] As a PET tracer, ^{11}C-labeled flumazenil has been successfully used in live animals and human brain.[86,201,38]

[^{11}C](+)3- and [^{11}C]4-NMPB and mACh receptors. NMPB (N-methyl-4-piperidylbenzilate) is a muscarinic acetylcholine (mACh) receptor antagonist. The mACh receptors belong in turn to the family of receptors that are coupled to GTP-binding protein (G-protein), and it has an important role in memory and cognitive functions[29,100,101,174,87] as well as in cortical processing of sensory information,[171] and in control of regional cerebral blood flow.[222] [^{3}H]4-NMPB has previously been used *in vitro* in rodent brains[135,134] and has been recently labeled with carbon-11[177] for use as an *in vivo* PET imaging agent.[271] Since the cloning of five muscarinic receptor subtypes,[113] the direct characterization of individual muscarinic receptor subtype-ligand interactions has become feasible, thus facilitating the search for specific ligands for possible treatment, pharmacological investigations, or tracing purposes.[53]

[^{11}C]cyano-dizocilpine and NMDA-subtype glutamate receptors. [^{11}C]Cyano-dizocilpine is a PET tracer developed on the basis of dizocilpine (previously MK-801), a non-competitive antagonist of the N-methyl-D-aspartate (NMDA) subtype of the glutamate receptor,[5] and it shows reversible and saturable binding.[260] Dizocilpine blocks NMDA responses in a voltage-dependent manner,[112] and the blockade of the binding sites is use-dependent,[261] suggesting close association between the binding sites and the ion channel in such a manner that when the opening of the channel occurs these binding sites are uncovered.[132] To allow the influx of calcium and sodium into the cell as a consequence of the binding of the excitatory amino acid glutamate, an internal voltage-dependent blockade of the channel by magnesium ion must be overcome.[158] The opening of the ionophore is facilitated by the binding of glycine[133] and modulated by the binding of polyamines[209] and zinc.[266] The presence of an agonist increases the binding of radioligands to a phencyclidine (PCP) recognition site,[147,61] which is identical or closely related to the binding site for dizocilpine. L-Glutamate and glycine alone, or even more in combination, increase by several fold the affinity of [^{3}H]dizocilpine for the NMDA receptor.[209] The widely distributed NMDA receptors have been well mapped previously by tritiated dizocilpine binding to rat brain membrane preparations[260] and by autoradiography.[19,217] The later discoveries about the neurobiology of the NMDA receptor and the earlier studies by Olney and colleagues[194,195] that led to the concept of excitotoxicity stimulated a search for tracers that could be used for studying the pharmacology of glutamate toxicity *in vivo*. [^{3}H]dizocilpine uptake in ischemic tissue in a rat model of focal cerebral ischemia is eventually increased after waiting long enough for the nonspecific fraction to decrease.[254] At early times after dizocilpine administration, the majority (> 80%) of the label is not associated with the dizocilpine recognition site,[207] and that disturbs the noninvasive *in vivo* visualization of the specific binding to NMDA receptor. In the development of potential PET tracers for NMDA receptor activation, (±)[^{18}F]fluoro-methyl-dizocilpine was synthesized, but specific binding could not be visualized because of the type of anesthesia used during animal PET investigations, and because of the racemic nature of the particular tracer.[15] The (–)-isomer of dizocilpine is about 5-6 times less potent than the (+)-isomer.[260,207] The activation of NMDA receptors was shown with (+)-3-[^{125}I]iodo-dizocilpine in rat focal ischemia by *ex vivo* autoradiography[160] and with (+)-3-[^{123}I]iodo-dizocilpine in patients with cerebral haemorrhages[198] or Alzheimer's disease[22] examined by single photon emission tomography (SPET). Besides cerebral ischemia and haemorrhage, the excitotoxic mechanisms are thought to contribute to the neuronal loss that occurs after

cerebral trauma,[269] status epilepticus,[78,79] and hypoglycemic brain damage.[7] Another tracer, (S)-[N-methyl-^{11}C]ketamine, for activated NMDA receptors has been synthesised[88] and used successfully in human volunteers for studying receptor occupancy in relation to several central nervous system effects caused by subdissociative doses of (S)-ketamine.[89] However, in patients with medial temporal lobe epilepsy, no neurochemical activation of the NMDA receptor channels could be identified.[140] Only decreased binding was observed in epileptic tissue, with many possible explanations. Besides its involvement in Alzheimer's disease, NMDA receptor activation-induced neurotoxicity is proposed to play a role in the pathogenesis of other chronic neurodegenerative disorders.[169]

$C^{15}O_2$. For measuring regional cerebral blood flow (rCBF) *in vivo* with PET, a method that involves the continuous inhalation of cyclotron-produced ^{15}O-labeled carbon dioxide ($C^{15}O_2$) has been used.[63,239,122] $C^{15}O_2$ is converted in the lungs to $H_2{}^{15}O$; and after 6 to 8 minutes of inhalation, an equilibrium is achieved in the brain, wherein delivery of $H_2{}^{15}O$ to the brain is counterbalanced by tracer washout and physical decay of the radionuclide ($t_{½}$=123 seconds). The regional tracer concentration at equilibrium is dependent on the rate of blood flow in the region, the arterial activity function, and the blood-brain partition coefficient of the tracer. The continuous (equilibrium) inhalation of $C^{15}O_2$ is suitable in subjects with intubated airways, though it imposes a higher radiation dose to lungs and total body, in comparison to the alternative, widely applied tomographic method for assessing rCBF, namely, the *in vivo* autoradiographic method after a bolus injection of $H_2{}^{15}O$.[110,69]

[^{99m}Tc]Hexamethylpropylene amine oxime (HMPAO). A lipophilic compound, HMPAO can be labeled with ^{99m}Tc and used as a tool for determination of rCBF *in vivo* by single photon emission computed tomography (SPECT).[188] Because of its lipophilicity, it crosses the blood-brain barrier freely, becoming thereafter less lipophilic and is trapped in the tissue for some hours. The distribution of [^{99m}Tc]HMPAO, reflecting the rCBF, correlates well with the distribution of microspheres and iodoantipyrine.[34,144,154]

2-deoxy-2-[^{18}F]fluoro-D-glucose (FDG) and D-[1-^{14}C]-glucose. An analogue of glucose that is used in the DG method, i.e., 2-deoxy-D-glucose, and glucose itself are competitive substrates for two initial steps of glucose utilization in the brain. The first step involves the bidirectional blood-brain barrier transport; and the second, the hexokinase-catalyzed phosphorylation of hexoses in the cerebral tissues. Deoxyglucose-6-phosphate (DG-6-P), once formed by hexokinase, is only minimally metabolized further, and is essentially trapped in the cerebral tissues (**Figure 1-3**). After a certain experimental time period, the brain and plasma precursor concentrations of DG drop to a low value, relative to the total radioactivity concentration in the brain; and the autoradiograms made at this time-point are the net result images of the relative rates of glucose utilization under the experimental time period in the structural components of the brain.[233] The DG method has been adapted for humans by the use of 2-deoxy-2-[^{18}F]fluoro-D-glucose (FDG) and PET.[203,210] To calculate the rate of glucose metabolism, an operational equation created by Sokoloff and co-workers (1977)[233] is used. In general, it is an equation (**Equation 1.6**) for the measurement of rates of enzyme-catalyzed reactions with tracers:

$$RCMRG = \frac{(C_t - C_e)}{LC \quad (I_p - K)} \qquad 1.6$$

In this equation the numerator represents the tracer metabolite concentration made up of $C_t - C_e$, where C_t is the measured total radioactivity concentration, and C_e, the brain precursor

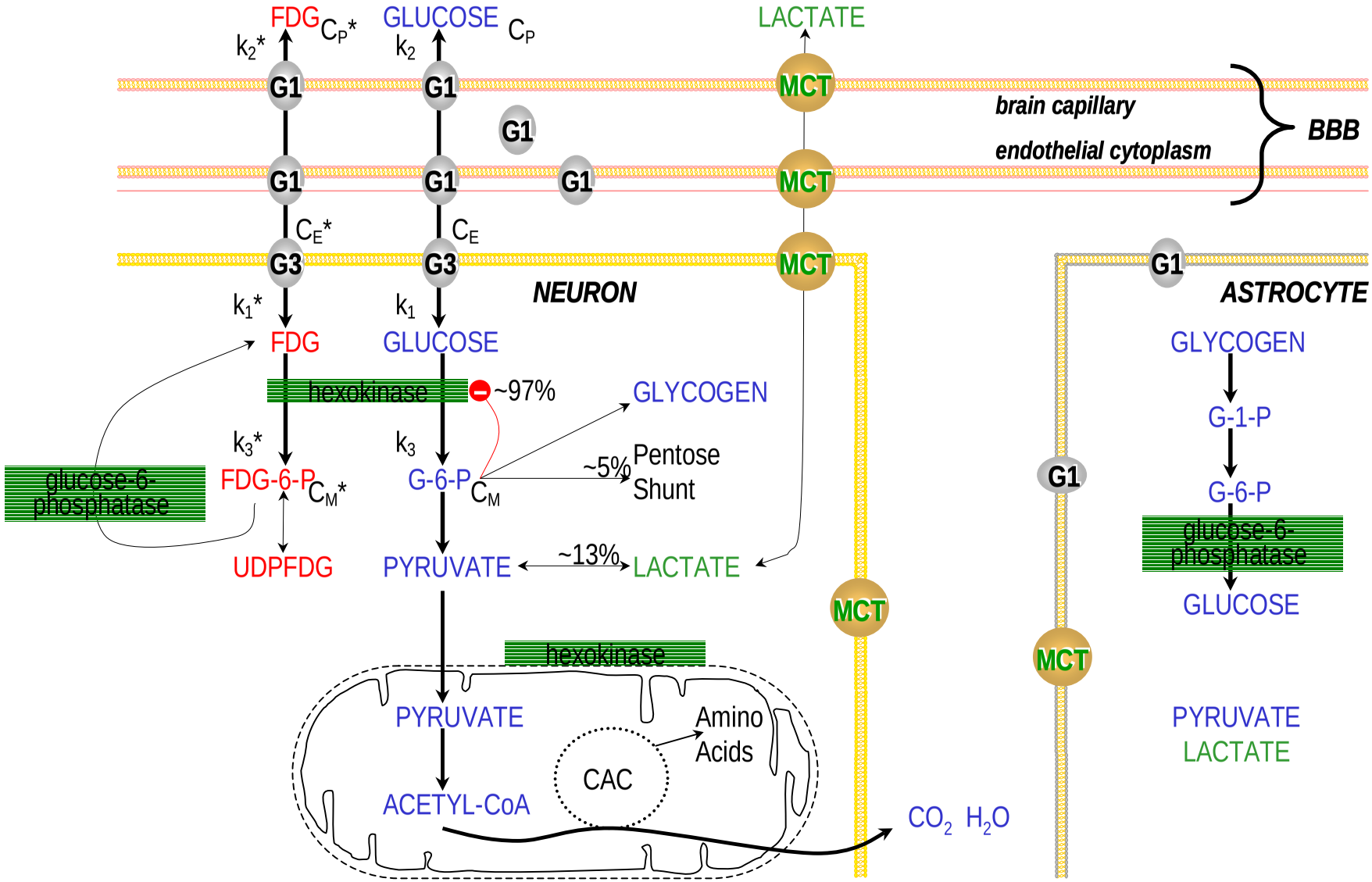

Figure 1-3. Glucose and deoxyglucose in brain tissue. Neuron (yellow), bloodvessel (red) and astrocyte (gray). C_p* and C_P, represent the concentrations of FDG and glucose in the arterial plasma, respectively; C_E* and C_E, represent their respective concentrations in the tissue pools that serve as substrates for hexokinase. C_M*, represents the concentration of FDG-6-phosphate in the tissue. The constants k_1*, k_2*, and k_3*, represent the rate constants for carrier-mediated transport of FDG from plasma to tissue, for carrier-mediated transport from tissue back to plasma, and for phosphorylation by hexokinase, respectively. The constants k_1, k_2, and k_3, are the equivalent rate constants for glucose. CAC, citric acid cycle; G1 and G3, are the predominant facilitative glucose transport proteins in the brain; MCT, the monocarboxylate transporters.

concentration. The denominator represents the integral of brain precursor specific activity multiplied by a factor, the lumped constant (LC). The integrated specific activity of the precursor is made up of $I_p - K$, where I_p, is the integral of plasma precursor specific activity, and K is the correction factor for the difference between the integrals of brain and plasma precursor concentrations. The experimental time period is recommended so that the impact from C_e and K is minimal. The LC and metabolic rate of glucose are inversely proportional to each other, and LC is necessary for relating the cerebral total radioactivity concentration to glucose metabolism. The LC does vary with the species of animal[234] and according to the pathological state.[197,240,127,236,237] It is, therefore, necessary to determine the LC in the pathological state investigated. Since the LC is not easily measured, one typically uses a value for normal whole brain and assumes that this value is valid in individual cases for the tissue of interest and speculates on theoretical grounds[42] as to how improbable it is that the LC would change in any particular experimental setup.[242,268,130,70,124]

Methods have been developed for measuring glucose utilization with labeled glucose itself, in which case no LC correction is neccessary, as the kinetics for transport and phosphorylation are the same for the tracer and the natural substrate.[148] The label passes through the glycolytic pathway and enters the citric acid cycle, where it is effectively trapped in intermediary metabolites associated with the cycle. The pentose shunt can remove the 1 carbon but its activity is thought to be low in the brain.[106] Though the labeled glucose method produces results that are similar to the values obtained with the deoxyglucose method,[142,93] the labeled glucose is not very popular. In **Panel 1-3** most important pros and cons of labeled deoxyglycose and glucose methods are listed. In order to study the behavior of FDG in experimental TBI, the present study compared the uptake of position-1 ^{14}C-labeled glucose with the uptake of FDG and the relative rCBF. Glucose and FDG have different kinetic characteristics for their respective passage across the blood-brain barrier (BBB) and for the enzyme, hexokinase.[71]

Panel 1-3: Characteristics of methods for determination of glucose utilization

Deoxyglucose method

- Long duration (30-45 min) needed for a favorable metabolite*/DG* ratio during which a steady state is neccessary for correct results
- Results are needed to transform to true values of glucose utilization with the aid of lumped constant
- Minimal loss of DG-6-P

Labeled glucose method

- Only short times (5-10 min) are possible for a favorable metabolite*/Glucose* ratio
- Loss of label via CO^*_2, lactate* or pentose shunt
- Identical kinetics of the tracer to the substrate of interest

***** radioactive label

1.4 Traumatic brain injury

Head injuries are present in more than half of trauma-related deaths, and accidental injury is the leading cause of morbidity and mortality among children and young adults in the developed world.[255] Two accepted concepts on which modern treatment of head injury is based are that not all neurological damage occurs at the time of impact and that the injured brain is much more sensitive than the non-injured brain to alterations

Panel 1-4: Traumatic brain injury

Primary injuries

- Rapid acceleration or deceleration
- Contusions, bruises
- Shearing/tearing and rupture of tissues
- Hematomas and blood clots

Delayed secondary injury

- Increased intracranial pressure
- physiological, biochemical and vascular abnormalities

in physiology.[41,121] In other words, much of the ultimate neuronal loss may be caused not by the injury itself, but by an uncontrolled vicious cycle of biochemical events set in motion by the trauma (**Panel 1-4**). The control of this complex cascade remains one of the most important challenges in the acute management of brain injury. Procedures that minimize this damage can improve the prognosis of the patient who has sustained a traumatic brain injury.

The brain trauma model and glucose metabolism

Experimental models of traumatic brain injury (TBI) try to recreate reproducible, graded and quantifiable brain injury for the evaluation of potential and clinically relevant neurochemical correlates coupled with the monitoring of the response to pharmacologic interventions. Among the diversity of experimental TBI's (including cerebral cortical contusion,[190,57,49] and head acceleration[67,156,157]) the method of injecting physiological saline into a closed cranium, termed fluid-percussion injury (FPI), is one of the most widely used and well characterized models,[163,48] one that reproduces some aspects of the biomechanical, physiological, neurological, and pathomorphological responses observed in human closed head injury. The FPI method enables the reproducibility of a mild, moderate, or severe level of brain damage, assessed in terms of neurological outcome and dependent on the magnitude of the impact (>1, 1.5-2.0, and 2.5-3.6 atm, respectively).[163] The immediate transient hypertensive response was more significant and prolonged at higher levels of injury and was followed (only in case of high-grade injury) by a significant decrease in mean arterial pressure.[163,241] The post-injury suppression of electroencephalographic amplitude correlated with the degree of injury and could be observed in both injured and uninjured hemispheres.[48] Neurological dysfunction after FPI is related to the level of injury, the highest degree of neurological impairment being demonstrated by the animals injured at the highest levels of impact.[163,48] The presence of neuronal injury, as identified by alterations in morphology and affinity for acid fuchsin[33] and silver stain, was demonstrated from as early as 10 min for up to 7 days after a moderate level (2.2 atm) of lateral FPI.[102] The frequency of injured neurons was greatest in the ipsilateral cortex, hippocampus, and thalamus. A loss of Nissl-stained neurons was observed in these regions beginning at 12 hrs after the FPI.[102,44] Highly selective and irreversible neuronal injury was seen in ultrastructural analysis of the hippocampus 15 min after moderate FPI.[45] There is evidence of initial global, with persistent regional, decreased blood flow at the site of moderate-level FPI.[264,263,46,47] Although these reductions in cerebral blood flow alone do not appear to be sufficient to explain the neuronal injury in corresponding brain areas[6] within the context of brain trauma, some neurons exhibited increased sensitivity to secondary ischemia.[121] Disruption of the blood-brain barrier (BBB) was dependent on the injury level. At a low level (< 1 atm) the BBB is reestablished in most brain regions at 60 min postinjury;[65] whereas at a moderate level of FPI, the BBB breakdown was most prominent at 6 hrs postinjury,[33] and mechanical damage to vessel walls was seen by ultrastructural observation of the trauma-site cortex.[45] After high-grade (~ 5 atm) FPI, the BBB breakdown was bilateral up to 24 hrs after the trauma, at which time the abnormal permeability became restricted to the impact site.[248] The local cerebral metabolic rate of glucose (LCMRG) after experimental traumatic brain injury (TBI) was previously measured with [^{14}C]deoxyglucose (DG) by using the method involving rate constants, and lumped constant developed[233] for normal animals. The assumption has routinely been made that the use of the DG method following TBI yields results that are both valid and reliable. Previously, the uptake of DG administered 10 or 20 min before experimental concussion, which produced immediate transient loss of consciousness associated with transient apnea, was similar to that of the

control animals.[224] Decreased DG utilization has been measured in cats 1 hour after FPI[95,40] and in rats 4 and 24 hrs after moderate FPI.[43] On administration of DG 15 min after moderate FPI in rats, the LCMRG was significantly elevated bilaterally beyond the values from sham-controls in a variety of cortical and subcortical sites in a study performed by Ginsberg and colleagues[70] (1997). A phenomenon of decreased LCMRG at the injury site and a significantly increased LCMRG in other surrounding ipsilateral sites[242] or bilateral regions[124] of rat brain after FPI has been observed. In studies by Hovda *et al.*[107] (1990) and Kawamata *et al.*[130] (1992), a remarkably higher LCMRG was observed in the entire cerebral cortex and hippocampus, with the greatest increase in the hemisphere ipsilateral to the percussion site, in rats subjected to FPI than in sham-operated rats. Yoshino *et al.*[268] (1991) followed the changes in LCMRG with time and found marked increases in LCMRG immediately after FPI and a subsequent return toward control values by 6 hrs, followed by a decrease in LCMRG and spontaneous recovery over the course of 10 days. The changes were seen primarily within the hemisphere ipsilateral to the site of the FPI. In another study, LCMRG was shown to be continuously decreased at 6 and 24 hrs and 2 weeks after the injury.[124] The oxidative metabolism following lateral FPI was shown to be increased acutely[253] and later after the injury, to be depressed for several days, primarily within the cerebral cortex and hippocampus ipsilateral to the site of injury.[108] FPI produces also expression of neuronal stress proteins and immediate-early genes,[208] cognitive dysfunction,[229] and, as demonstrated in cats, a reduction in cerebrovascular responsiveness to changes in pCO_2,[256] loss of pressure autoregulation,[146] and increases in intracranial pressure and oedema.[219]

PET in traumatic brain injury

Although the usefulness of PET in quantifying *in vivo* hemodynamics and metabolism is generally recognized, there have been only a few PET studies on head injury.[2] One can expect an increasing use of functional imaging by PET in modern rehabilitation and treatment research on traumatic brain injury.[3] PET using FDG has identified a decreased glucose utilization within 4 – 20 days postinjury in patients having recovered consciousness.[141] Similarly, decreased regional glucose utilization as measured with FDG was seen in children at a median period of 53 days after severe brain injury,[262] and in adults 3 – 12 months after mild-moderate head injury.[115] The PET results were not better predictors of clinical outcome than other methods used.[262] In the acute phase (within 10 days) of traumatic brain injury a discordance between FDG uptake and cerebral blood flow (CBF) has been shown: The CBF was reduced in all patients, but in one patient with severe traumatic brain injury [the Glasgow Coma Scale (GCS)[249] score 4 under PET FDG investigation] the cerebral metabolic rate for glucose was elevated,[265] whereas in another patient[1] with mild traumatic brain injury the FDG uptake was normal. Higher initial cerebral FDG uptake as compared with a subsequent decreased uptake has been measured acutely (2-4 days) by FDG PET after severe head injury in patients with GCS scores of 4 –7.[109] Acutely after severe traumatic brain injury, the cerebral metabolic rates for oxygen ($CMRO_2$) were normal, with a subsequent significant fall between the first and third days after injury (GCS $\leq$ 8, not a PET study).[225] Decreased regional $CMRO_2$ was also measured by PET 10 days after severe brain trauma, and the metabolic ratio ($CMRO_2$ / CMRG) in the same study was decreased, suggesting anaerobic glycolysis.[265] In a recent study different techniques were mixed in comparing global values from arteriojugular measurements of cerebral oxygen consumption with cortical values of glucose consumption measured by FDG PET; and a decreased metabolic ratio was found in 56% of the patients studied within

the 1st week of severe traumatic brain injury.[12] The authors called this shift between metabolic rates of oxygen and glucose "cerebral hyperglycolysis". There are no studies available in which an *in vivo* PET investigation on neurotransmission after traumatic brain injury has been conducted.

Glutamate-, ACh-, and GABAergic neurotransmission in brain trauma

The pathological changes associated with traumatic brain injury may be due, in part, to alterations in endogenous neurochemical systems, including those involved in normal neurotransmission. These events may include alterations in neurotransmitter synthesis, release, or re-uptake mechanisms or changes in pre- or postsynaptic receptor activity (for excellent reviews, see McIntosh and co-workers).[166,167] It is often difficult to determine what is the cause and what is the effect of a neurological malfunction. PET could be one of the few methods that would enable the assessment of the functional state of neurotransmission *in vivo*.

Both experimental[128,191] and human[24,202,105] traumatic brain injuries induce an acute and potentially neurotoxic increase in extracellular glutamate. Clinical data contradictory to most of the data on experimental traumatic brain injury show that glutamate concentrations may be elevated for a long time period. Pretreatment with noncompetitive NMDA antagonists attenuates neurological motor deficits,[94,165] enhances the recovery of memory performance[204] and cognitive outcome,[230] improves brain metabolic status and postinjury decline in magnesium concentrations,[54] and decreases contusion volume and hemispheric swelling[138] following experimental TBI. Also, postinjury treatment with magnesium salts as indicated by decreased magnesium concentrations[252] has been shown to cause an improvement in neurological motor and cognitive deficits and decreased regional cerebral edema formation[162,164,96] after TBI. Beneficial effects on behavioral dysfunction and on cortical lesion volume have also been obtained with modulation of glycine[231] and polyamine binding sites[251] in NMDA receptor-ionophore complexes. A more recent approach to reverse glutamate-induced neurotoxicity following traumatic brain injury is the use of presynaptic glutamate release inhibitors.[170] Only Miller and coworkers[173] have so far investigated the fate of NMDA subtype glutamate receptors after experimental traumatic brain injury. They found an acute decrease in NMDA receptor binding in both cortex and hippocampus.

Research data suggest an immediate cholinergic hyperfunction in the acute posttraumatic period followed by a hypofunctional cholinergic state later after injury.[215,216,84,205] Early anticholinergic treatment with scopolamine attenuated motor deficits.[149] Postinjury administration of cholinergic agonists improved cognitive function,[205] whereas blockade of the cholinergic system resulted in cognitive impairment in rats following traumatic brain injury.[51] A prolonged reduction in the evoked release of hippocampal and cortical acetylcholine (ACh)[50] and reduced immunohistochemical staining of ChAT neurons[75,39] have been shown after traumatic brain injury. FPI induced a prolonged increase in the maximum number of mACh binding sites in the hippocampus and cerebral cortex.[123,37] Loss of cholinergic neurons was seen in the rat brain following TBI.[220] Also, cholinergic agonists attenuated the decrease in forebrain choline acetyltransferase (ChAT) immunoreactivity following FPI.[206]

The $GABA_A$ ergic neurotransmission, which might be a major counterbalance to the excitotoxic mechanisms, has been only minimally investigated in experimental traumatic brain injury. A reversible increase in extracellular GABA concentration was shown by microdialysis in ischemia in both rat[103] and human[104] brains as well as in concussive brain

injury in rats.[191] The depressant diazepam was able to protect against ischemic damage.[221] Recently, improved effects on mortality and cognitive outcome were observed in rats subjected to moderate-level FPI when the animals were pretreated with diazepam.[193] Postinjury treatment did not enhance the survival but induced significantly better recovery of cognitive function.

2. AIMS OF THE THESIS

The principal goal of this thesis was to develop and validate methods for *in vitro* evaluation of positron emission tomography tracers, with application to experimental neurotrauma. Studies toward this goal included:

- Investigation of the suitability of the storage phosphor imaging system for working with high-energy positron emitters, for example for receptor binding in tissue homogenates and quantitative frozen section autoradiography (I, II).

- The development of methods usable for characterizing newly labeled receptor ligands with potential for application in positron emission tomography investigations on research animals or on humans (III, IV).

- The characterization of PET tracers in a biological model, i.e., experimental neurotrauma by using established *in vitro* and *ex vivo* methodology (V, VI).

3. MATERIALS AND METHODS

3.1 Radiation detection systems

Storage Phosphor (SP) plates, (Molecular Dynamics, USA; 20 x 25 cm) were used as one means of measuring radioactivity. Radioactive contamination of the plates was removed by using Intensifying Screen Cleaner (Kodak, New York, USA). Before and after use, background noise and remaining signals were erased by exposing the SP plates to an Image Eraser (Molecular Dynamics) for at least 6 min. For exposure the samples were placed on an SP plate (which was covered with a plastic foil) and pressed against it by means of a Molecular Dynamics Exposure Cassette. After exposure of the plate at room temperature for the desired time, a Phosphor Imager (Molecular Dynamics) was used to scan the plate with a laser beam. Pixel sizes from 50 μm and upwards were chosen depending on conditions of the experiment. The scanning operations, as well as data display and analysis, were performed by using the software ImageQuant (Molecular Dynamics). For quantitative analysis, after volume integration of the regions of interest (ROI), the radioactivity was expressed as the sum of all pixel (picture element) values minus the local background level close to each object. In other applications, the average pixel value after backround subtraction was used. The individual calibration standard was composed of a dried drop of 20 μl of tracer-solution on thin absorbent paper. The standards were prepared for each SP plate. The **γ-counter system** consisted of four scintillation counters (NaI(Tl), diameter and height = 75 × 75 mm) of the well type (diameter and depth 28 × 55 mm) in a 6-cm-thick lead shield. The amplified pulses were analyzed by a low level discriminator and counted by computer interfaced scalers. Each sample was measured usually for 30 sec, unless stated otherwise; and results were decay corrected. **Radioactivity from ^{3}H and ^{14}C** was counted in a liquid scintillation system (LS 6000 series) using Ready Organic™ liquid scintillation cocktail (Beckman Instruments Inc. Fullerton, CA, USA).

3.2 Radiotracers and other chemicals

All tracers (excl. D-[1-^{14}C]-glucose, [^{3}H]NMS and [^{99m}Tc]HMPAO) were produced by the staff chemists at the Uppsala University PET Centre and were used either for the present work only or shared in parallel with use in other projects. $^{11}CO_2$ was produced by the $^{14}N(p,\alpha)^{11}C$ nuclear reaction using a cyclotron Scanditronix MC-17. [N-Methyl-^{11}C]flumazenil was synthesized according to standard procedures.[159] The synthesis of (+)-3-[^{11}C]cyano-dizocilpine was achieved by reaction of (+)-3-iodo-dizocilpine with hydrogen [^{11}C]cyanide in the presence of tetrakis-(triphenylphosphine)-palladium(0) [Pd(PPh3)4].[5] The [^{11}C](+)3- and [^{11}C]4-NMPB's were obtained after conversion of [^{11}C]carbon dioxide to [^{11}C]methyl iodide, which was then used in an N-alkylation reaction of the corresponding N-desmethyl compounds.[177] The concentrations of ^{11}C-labeled tracers were calculated from calibration curves by simultaneous monitoring of radioactivity, UV absorbance, and mass (HPLC), with authentic substances used as standards. The mean (± SEM) specific radioactivities at the start of sample exposure were 721 ± 120, 60 ± 18, and 28 ± 4 MBq/μmol for [^{11}C]cyano-dizocilpine, [^{11}C]flumazenil, and [^{11}C]4-NMPB, respectively. ^{18}F was produced by the ^{18}O (p,n) ^{18}F nuclear reaction, and [^{18}F]Fluorodeoxyglucose (FDG) was prepared by routine procedures (FDG MicroLab unit, GE Medical Systems, Milwaukee, WI, USA). [^{99m}Tc]Hexamethylpropylene amine oxime ([^{99m}Tc]HMPAO) was

prepared by mixing a vial of HMPAO (Ceretec™, Nycomed Amersham plc, UK) with 5 ml (30 MBq/ml) of pertechnetate ($^{99m}TcO_4^-$) kindly provided by the members of the Department of Nuclear Medicine at Uppsala University Hospital. D-[1-^{14}C]-glucose was bought from NEN™ Life Science Products, Inc. (Boston, Massachusetts, U.S.A.), and l-[N-methyl-^{3}H]Scopolamine methyl chloride ([^{3}H]NMS) was purchased from Amersham Pharmacia Biotech AB (Sweden).

Flumazenil was kindly provided by La Roche (Switzerland). Zolpidem, triazolam, (+)- and (–)-dizocilpine, atropine sulphate, and pirenzepine were obtained from Research Biochemicals International (USA); and diazepam, L-glutamate, and glycine, from Sigma, (USA). Green mamba (*Dendroaspis angusticeps*) venom (0.5 g) was purchased freeze-dried from Miami Serpentarium Laboratories (USA); and ketamine, from Parke-Davis (Spain).

3.3 Animals

Male Sprague-Dawley rats and rhesus monkeys were used. The rats, weighing 200 to 450 g, were habituated to the housing conditions for at least seven days after arrival. They were housed at a constant temperature (20°C) and humidity (50%) and maintained under a 12-h light/ 12-h dark cycle, with lights on from 7:00 a.m. to 7:00 p.m. and given free access to laboratory animal chow and water. The rats were sacrificed by decapitation after a short exposure to diethyl ether[I] or CO_2.[II,III,V,VI] **Rhesus monkeys** (*Macaca mulatta*), weighing 7.0 - 11.2 kg, were used from the Primate Laboratory of Uppsala University PET-Centre. All studies with research animals were approved by the Animal Ethics Committee of Uppsala University.

3.4 Homogenates of transfected cells

Human mACh receptors (m1-m5), transfected in CHO-K1 cells were obtained from Receptor Biology, Inc. (Beltsville, USA). For the experiments the membranes were thawed and diluted in phosphate-buffered saline, pH 7.4 (PBS), and homogenized in a glass vessel with the aid of a Teflon pestle. The final concentration of receptors in the assay was in the range of 5.0 - 10.0 × 10^{-11} M.

3.5 Receptor binding in homogenates

For **preparation of rat brain P_2-fraction**, the forebrains were rapidly removed and homogenized in 10 tissue volumes of 0.32 M sucrose at 4ºC with a Polytron homogenizer PT 3000 (Kinematica, Littau, Switzerland) twice for 30 sec at setting 20. After centrifugation of the homogenate at 1240 *g* for 10 min at 4ºC (J2-MC-Centrifuge, Beckman, USA), the pellet (P_1) was discarded; and the supernatant (S_1) was further centrifuged at 19800 *g* for 20 min at 4ºC. The pellet P_2 was resuspended with a vortex mixer (Mistral, LAB-Line Instruments, Plaza) in 10 volumes of 50 mM Tris-HCl (pH 7.4) and kept on ice until used. For the saturation studies in paper III, the **P_6-fraction was prepared** by resuspending the P_2-fraction in 10 volumes of 50 mM Tris-HCl buffer (pH 7.4) without additional glutamate and glycine, and was further centrifuged at 39800 *g* for 20 min. The pellet (P_3) was resuspended and homogenized in 10 volumes of 50 mM Tris-HCl with the Polytron homogenizer for 30 sec at setting 20. This last washing step was repeated four times, and the final pellet (P_6) was stored at –70°C for not more than 2 weeks before use. On

the day of assay, the P_6-pellet was resuspended and homogenized again as described above in 50 mM Tris-HCl, pH 7.4. The **protein concentrations**[I,II,III] were determined by the bicinhoninic acid protein assay (Pierce, Rockford, USA) with bovine serum albumin as a standard.[232] **Ligand depletion experiments**[I] were performed as centrifugation assays to measure the free ligand concentration. Duplicates of P_2-fractions with different protein concentrations were incubated with [^{11}C]flumazenil. For termination of the binding reaction, the samples were centrifuged; and aliquots (1.0 ml) of the supernatants were measured in a γ-counter and compared with the sample without P_2-fractions. For the Phosphor Imager measurement, 20-µl aliquots of the supernatant on a BenchGuard sheet were used. For the **association** study,[I,III,IV] homogenates were incubated with tracer at 22ºC[I,IV] or at 37ºC.[III] The binding was started at different time points in reverse order and terminated simultaneously in all samples at time zero. In all binding studies (excl. depletion studies), the incubation was terminated by rapid filtration through Whatman GF/B glass fiber filters (FPB-148, fired, Gaithersburg, USA). For the **dissociation** study, the association of samples was terminated after 30,[I] 50,[IV] or 60[III] min; and dissociation was started by adding unlabeled competitor in excess at different time points, and the reactions were terminated simultaneously in all samples at time zero (of the dissociation reaction). In **ligand saturation experiments**,[I,III] the homogenates were incubated with increasing concentrations of tracers (0.3 to 50 nM[I], or 0.3 to 153 nM[III]) at 22ºC[I] or 37ºC[III] for 30[I] or 40[III] min. Nonspecific binding was obtained by incubation of adjacent samples with an excess of unlabeled competitor. In paper III saturation was studied under two conditions: first, 50 mM Tris-HCl, pH 7.4; and second, 50 mM Tris-HCl containing 1 mM L-glutamate and 30 µM glycine, pH 7.4. After termination of the incubation the filters were rinsed four times with 2 ml of ice-cold incubation buffer each time. Thereafter, the filter rings were collected from the cell-harvester (48 samples, Brandel, Gaithersburg, USA) and were transferred into vials for counting in a γ-counter[I,III,IV] and thereafter exposed to an SP plate in a cassette.[I] For assessment of the **specificity** of [^{11}C]flumazenil[I] and [^{11}C]cyano-dizocilpine[III] binding, the homogenates were incubated with a single concentration of the tracer and increasing concentrations of competitors. The incubations were performed at 22ºC[I] or 37ºC[III] for 30[I] or 40[III] min and terminated as described above.

3.6 Frozen-section autoradiography

In general, frozen sections were cut with a cryostat microtome and mounted on gelatin-coated glass slides. For **qualitative imaging**,[III,IV] the sections were preincubated in the incubation buffer at 37ºC and thereafter incubated with single concentrations of tracers for 50[III] or 40[IV] min at 37°C. The nonspecific binding was measured in the presence of excess blocker ((+)dizocilpine [III] or atropine[IV]). Thereafter the sections were washed twice for 5 min each time with the incubation buffer and dried under a stream of warm air (40ºC). The sections were exposed for at least 40 min to SP plates. The rat brain anatomical structures in autoradiographic images were visually identified according to the atlas of Paxinos and Watson (1982),[200] and for monkey brain according to that of Riche and colleagues (1988).[213] **Quantitative autoradiography**[II,VI] was performed in general as discussed earlier.[139] Coronal or sagittal sections of various thicknesses[II] or with a defined thickness of 10 (for [^{11}C]4-NMPB) or 20 µm (for [^{11}C]cyano-dizocilpine and [^{11}C]flumazenil)[VI] were mounted on gelatin-coated glass slides, dried at room temperature, and stored at –20°C until used for experiments within two to three weeks. For the treatment of the sections in paper II, the conditions described by Kloog and co-workers[135] were used with minor modifications. The

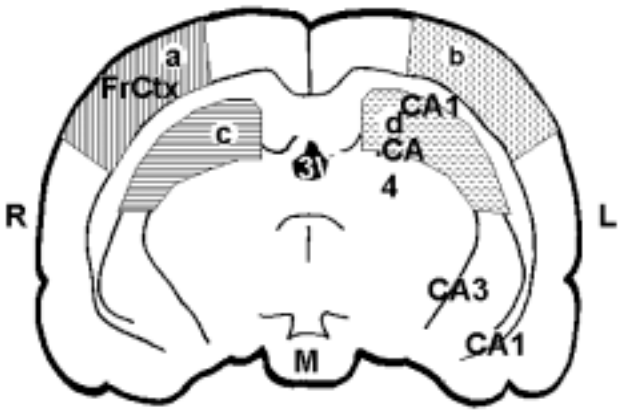

Figure 3-1.

Diagram showing some anatomical structures with typically investigated regions of interest (ROIs) in a coronal cryosection made at the level of 5 mm posterior to bregma. **CA1** – **CA4**, fields 1-4 of Ammon's horn, hippocampus; **3V**, third ventricle; **FrCtx**, frontoparietal cortex (trauma site); **L**, left; **R**, right; **M**, medial mammillary nucleus; **vertical lining** (**a**) and **dashed vertical lining** (**b**), trauma-site cortex and corresponding contralateral ROI, respectively. **Horizontal lining** (**c**) and **dashed horizontal lining** (**d**), trauma-side hippocampal ROI underlying trauma-site cortex, and corresponding contralateral hippocampal ROI, respectively.

sections were incubated in modified Krebs-Henseleit buffer (pH 7.4). In paper VI, 50 mM Tris-HCl, (pH 7.4) served as the incubation buffer. Sections were preincubated for 15 min. No preincubation was applied to sections used for [^{11}C]cyano-dizocilpine studies in paper VI. To define the total binding, the sections were incubated at different concentrations of tracers ranging from 0.05-60 nM in the incubation buffer at 24°C[VI] or 37ºC[II] for 40 ([^{11}C]cyano-dizocilpine and [^{11}C]flumazenil) or 50 min ([^{11}C]4-NMPB). Non-specific binding was determined in adjacent sections incubated in the presence of 1 μM (+)dizocilpine (for [^{11}C]cyano-dizocilpine), 1 μM flumazenil (for [^{11}C]flumazenil), or 10 μM atropine (for [^{11}C]4-NMPB). After the incubation, the sections were washed twice for 5 min ([^{11}C]cyano-dizocilpine and [^{11}C]4-NMPB) or 1 min ([^{11}C]flumazenil) each time with the incubation buffer and dried under a stream of warm air. For quantification, individual calibration standards were prepared for each set of brain sections and exposed to the same imaging plate. The standard was a 20-μl drop of tracer solution of known concentration placed on a thin absorbent paper (BenchGuard, Bibby Sterlin Ltd, UK), and exposed simultaneously with the brain sections. Knowing the concentration and volume of the standard sample, the amount of substance expressed in fmol was calculated. The total counts over the standard, measured by the SP imaging system, allowed the calculation of a calibration factor in counts/fmol. The signal measured for a region of interest (ROI) in a structure of a brain slice was given as an average count/pixel. Knowing the pixel size, the value was recalculated to counts/mm^2; and using the calibration factor, it was further converted to fmol/mm^2 (and fmol/mm^3 to get a value independent of section thickness). Before this calculation, the average count/pixel of the background area close to the brain slices was subtracted from the average count of the ROI. For ***ex vivo* frozen section autoradiography**,[V] the brains were quickly frozen after decapitation of the rats, and coronal sections of 40-μm thickness were cut with a cryostat microtome and mounted on gelatin-coated glass slides. They were next dried at room temperature and exposed for 4 or 12 hrs (FDG or [^{99m}Tc]HMPAO, respectively) to SP plates. A simplified quantification model was used without integrating brain or plasma precursor specific activity and without determining the metabolic rate or blood flow in absolute values, but still providing values that can be used as a basis for conclusions. The FDG uptake and blood flow were quantified by normalizing the uptake pixel-value in the ROI to the administered volume of the tracer and the body weight of the animal (uptake × ml^{-1} × kg^{-1}). The following working equation was used: $C_R \times 10^6/[(C_S \times IV)/wt]$, where C_R is the average pixel value for ROI; C_S, the total sum of the pixel values in the standard; IV, the volume of administered tracer; and wt, the weight

of the animal. Each set of brain sections from one animal was matched with a calibration standard prepared as follows: from the same tracer solution injected into the animal, a drop of 20 µl was pipetted onto a thin absorbent paper and dried. Each standard was then exposed simultaneously to the same imaging plate as the brain sections of the single animal. The ROI's were delineated in the cerebral cortex through all layers at the trauma site (a, in **Figure 3-1**) and in the corresponding contralateral region (b), and over the trauma-side hippocampus (c) and corresponding contralateral hippocampus (d).

3.7 *In vivo* PET

After an overnight fast, and before transport to the PET centre, the monkeys were anesthetized with an intramuscular injection of ketamine (100 mg). At the PET centre, inhalation anesthesia with a gas mixture of isoflurane, N_2O, and O_2 (0.4, 70, and 30%, respectively), was used combined with intravenous atracurium (0.5 mg/kg/h) for muscle relaxation. Electrocardiography and central body temperature were monitored throughout the study. The first study with [^{11}C]cyano-dizocilpine on the day of the experiment was conducted at least 4 hrs after the induction of anesthesia with ketamine. Radioactive doses for each administration were around 50 MBq, with specific radioactivity of about 100 GBq/µmol. Studies were performed in PC 2048-15B and PC 4096-15WB positron emission tomographs (Scanditronix, Sweden) equipped with eight detector rings, giving fifteen transaxial slices interspaced at about 6.8 mm and affording a spatial resolution of about 4-5 mm. Attenuation correction was based on 10-min transmission scans using a rotating ^{68}Ge pin source. One 60-min study consisted of 22 consecutive measurements (time frames). Images were reconstructed for each time frame, and ROI's were delineated in frontal cortex, right caudate, thalamic nuclei, cerebellar cortex, and white matter according to a monkey brain atlas.[213] Radiotracer binding kinetics were estimated after standardization of radioactivity uptake for its physical decay and normalization to the body weight of the monkey and injected radioactivity. Attempts for blocking were performed by intravenous injection of a single dose of (+)-dizocilpine or ketamine (0.1 and 2.5 mg/kg, respectively) before a bolus injection of [^{11}C]cyano-dizocilpine.

In three monkeys the regional cerebral blood flow (rCBF) was also measured before every [^{11}C]cyano-dizocilpine study. rCBF was measured by steady-state inhalation of $C^{15}O_2$. Regional CBF values were correlated to [^{11}C]cyano-dizocilpine uptake values in order to assess the rCBF component in the [^{11}C]cyano-dizocilpine uptake.

3.8 Parasagittal fluid-percussion brain injury

Rats were anesthetized with an intraperitoneal injection of sodium pentobarbital 60 mg/kg; and following insertion of a venous catheter for tracer injection into the left external jugular vein, they were placed in a stereotaxic frame. The rectal temperature was kept between 37.0 and 38.0°C. Parasagittal fluid-percussion injury was performed as previously described.[163] A female plastic Luer-Lok connector-cylinder was fixed with dental cement (Germany) into the craniotomy hole over the right frontoparietal cortex. For avoidance of changes in brain temperature, a heating lamp was kept at a predetermined distance over the head. For administration of moderate-level fluid-percussion (2.4 to 2.6 atm) the rats were connected with the Luer-Lok cylinder via a short rigid tube to an injury device (USA). Subsequently, the Luer-Lok cylinder and securing dental cement were rapidly removed, the bone plate was

replaced, and the wound was closed. Sham-operated animals were equally anesthetized and surgically prepared but not injured.

3.9 Double-tracer studies

For double tracer studies, around 15 MBq of FDG was mixed in a 1-ml syringe with 0.2 MBq of [1-^{14}C]glucose and injected in an average volume of 0.8 ml into the venous catheter 3 min prior to FPI. The animals were decapitated 10 or 20 min after the injection of the tracer (**A**, in **Table 4-4**). In three animals the tracer-mixture was injected 11 hr and 50 min after the FPI and the animals were decapitated 10 min after the injection of the tracer-mixture (**B**, in **Table 4-4**). After decapitation, the brains were cooled down on ice; and regions of the FPI in the cortex, corresponding contralateral region, and both hippocampi were dissected. γ-Radiation of ^{18}F in the dissected samples (about 0.03 g) was measured with a γ-counter; and, thereafter, the samples were completely dissolved (about 48 hours) in 0.5 ml of tissue solubiliser (Biolute-S, Zinsser Analytic, Berckshire, UK) and radioactivity from ^{14}C was counted in a liquid scintillation system (LS 6000 series) using Ready Organic™ liquid scintillation cocktail (Beckman Instruments Inc. Fullerton, CA, USA). The radioactivity concentration in the samples was calculated as the standardized uptake value (SUV) by using the equation $SUV=(Bq_S/wt_S)/(Bq_{Tot}/wt_B)$, where Bq_S, is the radioactivity of dissected sample, wt_S, the weight of the sample, Bq_{Tot}, the total radioactivity given, and wt_B, the body weight of the rat. This standardization compares the organ radioactivity concentration to an assumed equal total body concentration.

3.10 Data handling

Receptor binding studies were analysed, and curves fitted using the weighted nonlinear curve-fitting program LIGAND (Radlig 4.0, Biosoft, McPherson[168]). Raw decay corrected data sets were computed first to obtain binding data in molar concentrations. The t test was used for calculations of statistical significance. The t test for independent samples was used for comparison of the binding constants and uptake values at the trauma site to corresponding values in sham-operated animals. For comparison to the contralateral side in the same animal, the paired t test was used; and differences were considered statistically significant when $P < 0.05$. A one-way ANOVA with the Tukey post test was used to calculate the significance of differences between the data obtained for the different mACh receptor subtypes.[IV] The data were presented as mean ± standard error of the mean (SEM), if not stated otherwise.

4. RESULTS AND DISCUSSION

4.1 Establishing *in vitro* receptor binding with PET tracers

For characterization of the biochemical parameters of new pharmaceuticals with potentials for diagnosis and therapy, it is essential to perform studies under conditions simpler than those encountered *in vivo*. In the present study, the *in vitro* characterization of ^{11}C-labeled receptor ligands designed for use in *in vivo* positron emission tomography has been demonstrated. Both, the Phosphor Image technique and γ-radiation counting were used, and

the data obtained were compared with each other and with the data in the literature. The characterization of the SP plates, originally designed for computed (X-ray) radiography,[235] is a prerequisite for the application of the Phosphor Image system for *in vitro* receptor binding experiments with the short-lived, high-energy β^+-emitting radionuclides. Basic requirements for the application of imaging plates are the uniformity of the phosphor-complex layer, **uniform detection of radiation** over the entire plate, linearity of the dynamic range, spatial resolution, and sensitivity. For 7 plates tested, 30 drops with radioactivity of 30 cps were distributed over each individual plate. The difference between the highest and the lowest signal in areas over each plate was less than 10%. Reasons for differences within one plate may be unevenness of the storage phosphor particle layer or of the filters used for exposure of the radioactive spots. The latter can be minimized by drying the drops on the filter before exposure. The deviation among the plates was found to be 9.4 ± 1.7 %. For investigation of the linearity of detection of β^+-emitters by the SP plates, 20-µl spots with increasing radioactivity (1-850 cps) of a ^{11}C-tracer were exposed for 60 min. A **strict linearity** was kept in the major part of the curve. At very low radioactivity levels (less than 7 cps, see inset in **Figure 4-1**), the linearity was disturbed by environmental background radiation. Considering the linearity, an accurate quantification of radioactivity is possible. The wide linearity range excludes the problem of overexposure.[125] The excellent linearity, previously documented for low-energy γ- and β^--radiation, is now also validated for β^+ particles. For **sensitivity** measurement a signal/noise-ratio (S/N-ratio) was defined as the quotient of the mean counts of radioactivity and the corresponding standard deviation for four different levels of radioactivity. For the highest radioactivity, the S/N-ratio of the γ-counter was 25 % higher, compared with SP plates, indicating that the γ-counter measurement technique is more suitable. After around one half-life of ^{11}C, both γ-counter and SP plates had the same S/N-ratios, and in further lower radioactivity range, (after 60 and 90 min from the initial, high radioactivity measurement), the S/N-ratio for the SP plates became twice the value of that of the γ-counter; thus providing one benefit for SP plates, i.e. higher sensitivity in the lower radioactivity range. The higher sensitivity of SP plates may be attributable to the high capture efficiency of SP plates and the formation of multiple active centers on the storage phosphor crystals (Molecular Dynamics). In the γ-counter, the

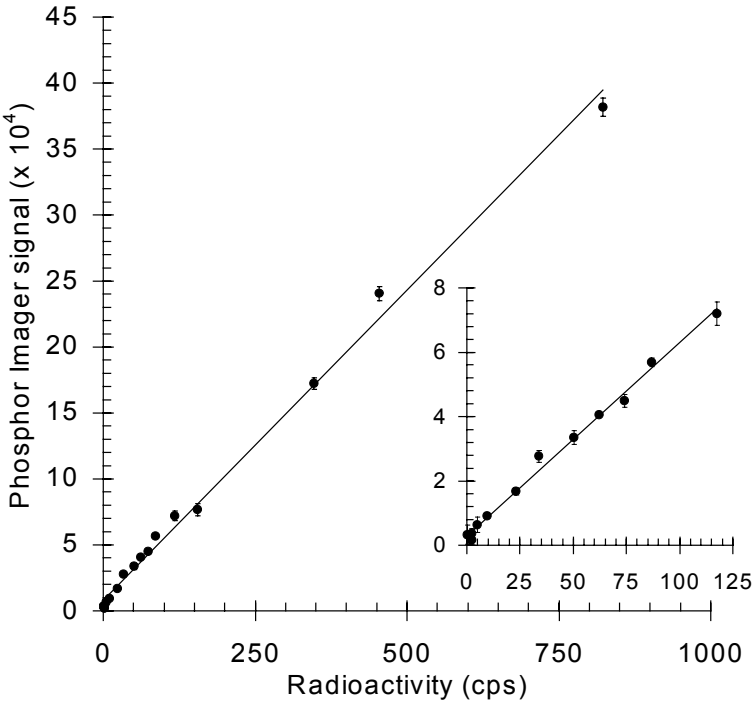

Figure 4-1. Linear dynamic range of the Storage Phosphor (SP) plates measured by integrating the volumes of radioactive spots from the exposure to 20 µl of ^{11}C-labeled tracer. Radioactivity was estimated with the γ-counter at the beginning of the exposure. The graph shows average values of 7 SP-plates with the standard errors of the mean (S.E.M). Inlet: Magnified view of low-level range.

iodine in the NaI(Tl)-crystal gives a high probability to obtain photoabsorption of the arriving γ-photons. For an increase in the efficiency of this type of detector, the crystal should be built thicker: but, thereby, the contribution of the background noise increases.[11] The **spatial resolution** gives information about the ability of the SP plates to distinguish between adjacent energy sources. Expressed as the full width of half maximum (FWHM), which is a suitable criterion for autoradiography,[125] the resolution appeared to be dependent on the orientation of the capillary pairs. The FWHM of capillaries mounted parallel or perpendicular to the long axis of a SP plate was found to be 566 μm and 650 μm, respectively. With exposure of ^{11}C to a film sensitive to high β-energy radiation, the FWHM is 180 μm.[36] The ^{11}C-nuclide emits a β^+-particle with a maximal energy of 1 MeV. The high energy involves a radiation length of several hundreds of micrometers in the phosphor-complex layer. β^+-particles from all directions make phosphor crystals active and are captured at nearly hundred percent, causing a larger area of latent image. There was no significant difference in resolution when the SP plates were scanned with different pixel sizes. The difference in the resolution depending on the axis of exposure might be caused by the laser beam reading the latent images in two directions, namely perpendicular ("fast") and parallel ("slow") to the long axis of the SP plate. In the direction of "fast " scanning, a delay occurs from reading to the transformation operation. The recorded pixels appear to be wider in the direction perpendicular to the long axis of the SP plate.[257]

In light of the above described properties of the SP plates, binding studies with the ^{11}C-labeled benzodiazepine ligand flumazenil were performed utilizing both SP plates and γ-counter system. Advantages and disadvantages of SP plates for quantitative autoradiography with short-lived PET tracers were explored by utilizing the muscarinic antagonist [^{11}C]4-NMPB. The *in vitro* validation of newly synthetized PET tracers by use of SP technology is becoming routine in PET or other imaging research facilities connected to PET.[226,120,118] Also other systems using SP technology have been validated for that purpose.[119] Instant imaging[66] or exposure to β-sensitive film[83] are other currently used alternatives to produce an image of ^{11}C radioactivity.

Receptor binding in homogenates

Flumazenil is a highly selective tool for studies of neuronal BZ receptors.[185,184,73] As a PET tracer, ^{11}C-labeled flumazenil has been successfully used in living animal and human brains.[86,201,38] Benzodiazepine receptors are well characterized; and their regional distribution in the brain and their pharmacological properties are well known,[183,20,238,245] making the comparison of obtained results with the literature data a valuable evaluation method. *In vitro* binding studies on benzodiazepine receptors have been done mainly with ^3H-labeled ligands and membrane fractions of different species.[20,136,211]

At the first step of the binding study, the **depletion** of the tracer ligand from the incubation medium was controlled. Within 10 % depletion, both the analysis of the binding curve and the model of nonspecific binding for use in non-linear, least-squares fitting of binding (as a function of the total ligand concentration) are valid.[114] The 10% depletion limit after incubation of 0.3 nM [^{11}C]flumazenil was similar for both measurement systems (0.11 ± 0.02 and 0.09 ± 0.01 mg of protein per ml assay medium as measured with SP plates and γ-counter, respectively). In the following binding studies, a protein concentration of less than 0.1 mg per ml assay medium was chosen. For better understanding of *in vivo* PET investigations and for characterization of receptor-ligand binding, the knowledge of **association and dissociation** kinetics are of high value. The [^{11}C]flumazenil binding

equilibrium of rat forebrain membrane fractions was reached within 5 min. The association half-time ($t_{½}$) was 9.0 ± 1.4 sec and 9.6 ± 1.8 sec, when measured with SP plate and γ-counter, respectively. A similar association constant (K_a), 1.72 ± 0.26 and 1.50 ± 0.31 nM^{-1} min^{-1}, and observed association rate constant (K_{obs}), 6.57 ± 0.98 and 5.78 ± 0.95, were obtained for both measurement systems (Phosphor Imager and γ-counter, respectively). In earlier studies, an equilibrium of the binding was obtained after 40 min of incubation of [^{3}H]flumazenil with P_2-fractions of rat cerebral cortex[184] and after 14 min in rat cerebellar membranes.[21] In both studies, the incubation temperature was 0º C, which might have slowed down the association rate.[114] In frozen sections of mouse brain at both 4ºC and 37ºC, the equilibrium for [^{3}H]flumazenil was reached in less than 30 min.[9] For a determination that the specific binding of [^{11}C]flumazenil was fully reversible, dissociation was induced by adding unlabeled flumazenil. The time for 50 % dissociation was 31.2 ± 3.0 sec and 34.2 ± 4.2 sec, (SP plates and γ-counter, respectively). The dissociation rate yielded 1.34 ± 0.11 min^{-1} and 1.25 ± 0.16 min^{-1} (SP plates and γ-counter, respectively). Brown and Martin[21] showed a dissociation rate of 0.118 min^{-1}, which is 10 times lower than in the present study. In *in vivo* studies, ^{11}C and ^{3}H-labeled flumazenil displayed both association and dissociation within 5 to 10 min.[201,86,73,35] The specific binding was saturable and amounted to 97 % of the total binding. **Saturation data** was best fitted to a single binding site model. SP plates and the γ-counter gave similar results for the dissociation constant (K_D): 2.0 ± 0.5 and 2.1 ± 0.2 nM, respectively, and for a total number of binding sites (B_{max}): 1.3 ± 0.2 and 1.7 ± 0.1 fmol/mg of protein, respectively. Looking at previous studies in which the K_D was found to be in the low nanomolar range and B_{max} to be a few picomoles per milligram of protein with the tritiated compound,[185,184,85] the validity of both types of measurements can be confirmed. Larger variations in results can be introduced because for each experiment, a new batch of tracer is synthesized and an individual concentration with its inherent measurement error is obtained. By use of a tracer labeled with a long-lived radionuclide, a single batch or a few batches can be used throughout a whole series of experiments. **Competition experiments** were performed using several BZ receptor ligands. The most potent displacer of [^{11}C]flumazenil was triazolam, with an IC_{50} value of 0.13 ± 0.01 nM. Unlabeled flumazenil, diazepam, and zolpidem were also potent displacers, showing IC_{50} values of 4.03 ± 0.75 nM, 26.4 ± 4.0 nM, and 36.9 ± 5.1 nM, respectively. Similar potency for flumazenil and diazepam in displacing [^{3}H]flumazenil in rat cerebral cortex[186] and human cerebral cortex[82] and for diazepam in rat cerebral cortex[184] has been shown previously. For zolpidem, an average IC_{50} value of 37 nM was obtained in different forebrain structures of mice.[9] In an *in vivo* study by Sanger and Benavides (1993),[218] the most potent displacer of [^{3}H]flumazenil binding in rat brain was triazolam, followed by diazepam and zolpidem, and this hierarchy corresponds with the ranking order of potency for these substances in the present study.

Receptor binding autoradiography, qualitative vs. quantitative

N-Methyl-4-piperidyl benzilate is a high-affinity muscarinic receptor antagonist.[135,134] The influence of the **cryosection thickness** on the strength of the phosphor imager signal was investigated at a thickness ranging from 10 to 125 µm. The slice thickness at which the signal reached its maximum was dependent on the concentration of the tracer. In the case of 0.5 nM [^{11}C]4-NMPB, the signal increased linearly until it reached a plateau at 25 µm; with 5 nM [^{11}C]4-NMPB, the plateau was reached at 50 µm. The maximal signal level differed 10-fold between these two concentrations, and also images with stronger signals were obtained with thicker cryosections. A linear relation between the thickness of sections from 5 to 14 µm has previously been demonstrated for a ^{125}I-labeled tracer.[247] This relationship shows that in frozen section autoradiography with PET tracers, it is possible to achieve a better signal and hence a better image by increasing the thickness of the slice in the range of 10 to 50 µm. This is not the case with ^{3}H-labeled tracers, where the very small penetration depth of the β^--particles constitutes a limitation. The association and concentration dependence of specific [^{11}C]4-NMPB binding were studied in the cerebral cortex and caudate putamen (striatum) in 10-, 25-, and 50-µm thick sections. Inspection of the **time-association** curve showed that equilibrium was reached only in the case of 10-µm-thick sections. In 25- and 50-µm-thick ones, the association and uptake process continued up to the end of the follow-up time, which, due to the fast physical decay of the ^{11}C radioactivity to a level close to the backround radiation, was limited to 50 min. In 200-µm-thick living brain slices incubated with 2 nM [^{11}C]4-NMPB, the binding equilibrium was reached after 100 and 130 min in rat cortex and striatum, respectively.[179] To evaluate binding at equilibrium in thicker slices and to determine the dissociation kinetics is thus practically difficult. The association would perhaps be faster, and hence the time for the tracer binding to reach the apparent steady state would be shorter, if a higher concentration of [^{11}C]4-NMPB had been used. Since lower concentrations of a radioligand take a longer time to equilibrate, a low concentration of radioligand was used for measuring how long it takes the incubation to reach equilibrium. The nonequilibrium effect of premature termination of the incubation is more prominent in low but not in high concentrations; therefore a shift appears from off-rate-limited to on-rate-limited kinetics in the low concentration range. Performing a Scatchard analysis of such data leads to overestimation of both K_D and B_{max}.[114] However, there is the reason to believe that also such possible factors as tracer diffusion within the tissue, local tracer concentration, and possible local depletion and modification by local

Panel 4-1: Successive steps in the quantification of receptor binding in quantitative frozen-section autoradiography with ^{11}C-labeled tracers

- Production of ^{11}C-labeled radiotracer and evaluation of its concentration (µg / ml)
- Standard dilution of the ^{11}C-labeled tracer with known concentration (nM)
- Preincubation, incubation, washing, and drying of the sections
- Preparation of the standard: a 20 µl drop of the standard dilution on a thin absorbent paper on athe non-slip coated side (e.g., BenchGuard)
- Exposing the cryosections together with the standard to a phosphor imaging plate. (One standard is necessary for each plate)
- Drawing a circular ROI over the image of the standard drop and computing the sum of all pixel values in this ROI. Calculation of the calibration factor in counts / fmol of ^{11}C-labelled tracer
- Converting the average counts / pixel in ROIs delineated in the images of the cryosections to fmoles / area (mm^2) or volume (mm^3) using the calibration factor and pixel size

nonspecific binding have their role to play in differences in ligand binding kinetics. This reasoning is supported by the observations of an eight-fold higher K_D for [^{3}H]QNB[68] and a twenty-fold higher K_D for [^{11}C]4-NMPB[179] for native brain slices than for homogenates; or the three to ten-fold difference in K_D for raclopride when comparing binding between human brain homogenates[81] and human brain *in vivo* by use of the PET technique.[55] Because the SP plates have superior sensitivity and a linear response over a wide radioactivity range, the **quantification** of receptor binding in fmoles/mm^2 (or per volume, that is, independent of section thickness) is a straight forward procedure (**Panel 4-1**). It is sufficient to include one concentration as a standard for calibration that should be exposed at the same time and to the same SP plate as the tissue sections. The specific binding in cortex and striatum in present work, appeared to be **saturable** over a concentration range of 0.05 to 12.8 nM of [^{11}C]4-NMPB. The Scatchard plots of the saturation data for 10-µm-thick sections were linear, suggesting a homogeneous population of binding sites in both regions examined. **Table 4-1** shows that the binding constants (K_D and B_{max}) in the two investigated brain regions depended on the thickness of the sections. B_{max} expressed in fmol/mm^3 was slightly higher in the striatum than in the cortex, but the increase with increasing section thickness was not statistically significant. The dissociation constant (K_D) was higher in thicker sections, indicating that factors other than ligand receptor interactions are involved. The K_D for [^{3}H]4-NMPB in cortex and striatum homogenates of mouse brain was 0.41 ± 0.03 and 0.38 ± 0.01 nM, respectively; and there appeared to be more binding sites in the striatum than in the cortex,[134] which is in good agreement with our results with 10-µm sections. There was a loss in tracer affinity in thicker sections. The average ratio between the binding capacity in cortex and striatum in sections of the three different thicknesses was 0.66 (with SEM ± 0.08), which means that the relative pattern of binding site distribution (i.e., **qualitative imaging**) was retained even if equilibrium was not reached in the thicker sections. The evaluation of quantitative binding parameters in this type of frozen-section autoradiography must be interpreted with caution, because the results might be influenced by experimental variables such as the thickness of the cryosections. The **general binding pattern** of the [^{11}C]4-NMPB autoradiograms in rat[II,IV] and monkey[IV] brains is in good agreement with the binding distribution of [^{3}H]4-NMPB in mouse brain homogenate preparations[134] and corresponds to previous reports of the distribution of muscarinic cholinergic receptors in human[32] and rat[64] brains. The binding pattern of [^{11}C]4-NMPB and the newly labeled [^{11}C](+)3-NMPB[244] in frozen-section autoradiography of monkey and rat brains was very similar.[IV]

Subtype specificity of [^{11}C]4-NMPB

Mulholland and co-workers[176](1988) developed ^{11}C-labeled N-methyl-4-piperidyl benzilate

Table 4-1. Scatchard plot analysis of saturation binding data of [^{11}C]4-NMPB by the use of autoradiography of frozen sections at different thicknesses. The data represented below are the mean (± SEM) of at least four independent experiments.

	Cryosection thickness					
	10 µm		25 µm		50 µm	
	Cortex	Striatum	Cortex	Striatum	Cortex	Striatum
K_D [nM]	0.49 ± 0.10	0.69 ± 0.15	1.12 ± 0.16	1.49 ± 0.31	1.93 ± 0.21	3.13 ± 0.44
B_{max} [fmol/mm^2]	1.01 ± 0.18	1.73 ± 0.37	3.07 ± 0.46	3.71 ± 1.26	8.68 ± 2.43	14.13 ± 4.24
B_{max} [fmol/ mm^3]	101 ± 18	173 ± 37	122.8 ± 18.4	148.4 ± 50.4	173.6 ± 48.6	282.6 ± 84.8

([^{11}C]4-NMPB) for use in PET; and with it, favorable kinetic properties in animals[23] and in human studies[271] have been demonstrated thus far. As, five distinct muscarinic receptors have been cloned, our interest in the subtype selectivity of [^{11}C]4-NMPB was evoked, especially in view of the principal importance of the availability of mACh receptor subtype-specific ligands for the characterization of the (patho)physiological roles of individual subtypes, how these can contribute to pharmacotherapies, and, last but not least, the discrete anatomical location of the subtypes. In connection with the quantitative autoradiography work,[II] a competition study was performed to investigate the subtype specificity of [^{11}C]4-NMPB. In five displacement experiments, pirenzepine and crude venom of the green mamba were used. Pirenzepine at 30, 300, and 3000 nM displaced the total binding of [^{11}C]4-NMPB by 15, 40, 60 %, respectively, in cortex and striatum, and by 0, 16, and 40 %, respectively, in the spinal cord in 10-µm-thick sections. When calculation was made from the displacement of ligand from muscarinic acetylcholine receptors by pirenzepine, it was found that 30 nM pirenzepine displaced a major part of the available M_1 subtype (83%) and that 300 nM pirenzepine displaced M_1 (98%) and M_4 (68%) muscarinic receptor subtypes.[116] The fact that 30 nM pirenzepine did not displace the [^{11}C]4-NMPB binding in the spinal cord but displaced about 15% of total [^{11}C]4-NMPB binding in the cortex and striatum suggested that the M_1 subtype is not present in the spinal cord, which is consistent with previous findings.[116] Only 15% of the total [^{11}C]4-NMPB binding in the cortex and striatum appeared to be accounted for by the M_1 subtype, which is abundant in these regions.[60] Pirenzepine at 300 nM displaced on average 16% of the total [^{11}C]4-NMPB binding in the spinal cord, apparently due to a block of a majority of the M_4 subtype. This suggestion is strengthened by the observation that 30 µg of protein/ml of crude green mamba venom, which is known at this concentration to block M_1 and M_4 subtypes,[60,126] displaced 13% of the total [^{11}C]4-NMPB binding in the spinal cord. The crude venom of the green mamba (30 µg of protein/ml) displaced the total binding of the [^{11}C]4-NMPB by 53, 60, and 13 % in cortex, striatum and spinal cord, respectively, in 10-µm-thick

Table 4-2. A) Properties of (+)3- and 4-NMPB binding to human m1-m5 subtypes of mACh receptors expressed in CHO-K1 cells. K_i, the equilibrium dissociation constant of unlabeled substances from competition binding experiments using [^{3}H]-N-methyl scopolamine as tracer; K_D, the equilibrium dissociation constant of corresponding ^{11}C-labeled tracers calculated from kinetic binding studies. **B)** Affinity profiles of (+)3- and 4-NMPB and corresponding ^{11}C-labeled tracers. > Denotes statistically significant difference with P<0.05 calculated by one-way ANOVA with the TUKEY post test. ≥ Denotes no significant difference.

A The equilibrium dissociation constants

mAChR subtype	Substance	K_i [nM]	K_D [nM]
m1	4-NMPB	0.26 ± 0.003	1.16 ± 0.32
	(+)3-NMPB	0.67 ± 0.09	0.67 ± 0.32
m2	4-NMPB	0.60 ± 0.02	0.25 ± 0.10
	(+)3-NMPB	1.40 ± 0.06	0.65 ± 0.44
m3	4-NMPB	0.35 ± 0.06	0.13 ± 0.03
	(+)3-NMPB	1.32 ± 0.21	0.11 ± 0.04
m4	4-NMPB	0.06 ± 0.004	0.07 ± 0.01
	(+)3-NMPB	0.27 ± 0.02	0.18 ± 0.03
m5	4-NMPB	0.36 ± 0.01	49.5 ± 16.6
	(+)3-NMPB	2.81 ± 0.20	1.09 ± 0.40

B The affinity profiles

[^{11}C]4-NMPB: m4 ≥ m3 ≥ m2 ≥ m1 > m5
4-NMPB: m4 > m1 ≥ m3 ≥ m5 > m2

[^{11}C](+)3-NMPB: m3 ≥ m4 ≥ m2 ≥ m1 ≥ m5
(+)3-NMPB: m4 ≥ m1 > m3 ≥ m2 > m5

sections. Since the mamba venom displaced approximately half of the [^{11}C]4-NMPB binding in the cortex and striatum and the effect of 300 nM but not that of 30 nM pirenzepine was in the same range, [^{11}C]4-NMPB was concluded to bind preferentially to the M_4 subtype of muscarinic acetylcholine receptor. A concentration of 3 μM pirenzepine further displaced the [^{11}C]4-NMPB binding, indicating an additional binding of [^{11}C]4-NMPB to M_2, M_3, and M_5 subtypes of the muscarinic acetylcholine receptor. The non-specific binding measured in the presence of 10 μM atropine ranged from 5 to 10 % of the total binding in all experiments. As shown later[IV] by the use of the five cloned human mACh receptors, the lowest equilibrium dissociation constant was obtained for the m4 subtype in kinetic studies [K_D, (K_{off}/K_{on})] 0.07 ± 0.01 nM, as well as in competitive binding studies [K_i, ($IC_{50}/(1 + [NMS]^*/K_D^*)$)][28] 0.06 ± 0.004 nM. The results from the kinetic binding data are presented in **Table 4-2**. The affinity profile for [^{11}C]4-NMPB (starting with the subtype for which [^{11}C]4-NMPB showed highest affinity) was: m4≥m3≥m2≥m1>m5 (> sign indicates significant difference with $P<0.05$, $F_{(4,10)}=8.7$). A binding profile for 4-NMPB from competition studies was m4>m1≥m3≥m5>m2 ($F_{(4,10)}=49.9$, results presented in **Table 4-2**). The K_D's for [^{11}C](+)3-NMPB did not differ significantly, thus exhibiting no selectivity for any subtype, whereas the binding profile of K_i's for (+)3-NMPB was m4≥m1>m3≥m2>m5 ($F_{(4,8)}=37.8$). The kinetic binding data of [^{11}C](+)3- and [^{11}C]4-NMPB and competition binding data of (+)3- and 4-NMPB showed that neither of these substances has an affinity profile that makes them suitable for subtype-specific assays. The largest difference in affinity was about 10 times (between m4 and m5 for 3-NMPB and between m2 and m4 for 4-NMPB). [^{11}C](+)3-NMPB similarly showed a low selectivity for the mACh receptors. [^{11}C]4-NMPB had slower kinetics than [^{11}C](+)3-NMPB, which influenced the possibility to obtain precise data to calculate K_D values for [^{11}C]4-NMPB. This phenomenon is particularly true for the association with and dissociation from the m5 subtype. In this respect [^{11}C]4-NMPB is similar to [^{3}H]-N-methylscopolamine.[60,59] Either [^{11}C](+)3- or [^{11}C]4-NMPB is suitable for PET studies of mACh receptors. Differential labeling of mACh receptors cannot, however, be anticipated.

[^{11}C]cyano-dizocilpine, a tracer only for in vitro use?

The **association** of 10 nM [^{11}C]MKC with its recognition site progressed at 37°C with a $T½_{ass}$ of 2.8 ± 0.3 min, and more than 95% of maximum specific binding was reached after about 20 min. The time for half dissociation $t_{½diss}$ was 9.0 ± 1.3 min, and about 65 % became dissociated during a 30-min period of observation. A longer time analysis of dissociation was practically difficult because of the fast decay of ^{11}C and the considerable decrease in specific activity in this type of experiment. Specific binding of [^{11}C]cyano-dizocilpine was **saturable** and best fitted to a single binding site model. The crude synaptosomal fraction was washed a total of four times in order to decrease the amount of endogenous glutamate and glycine and thereby lower the [^{11}C]cyano-dizocilpine binding. The affinity in extensively washed synaptosome fraction was increased in the presence of 1 mM L-glutamate and 30 μM glycine, from 10.1 ± 0.3 to 8.2 ± 0.4, without significant changes in B_{max} (about 1.7 pmol/mg protein), suggesting that the tracer bound preferentially to the activated form of the NMDA receptors. The binding of [^{11}C]cyano-dizocilpine was, however, less increased than shown previously for [^{3}H]dizocilpine,[259,61,209] [^{3}H]TCP,[147] or [^{3}H]FTCP.[58] As expected for the ranking order of potency,[258] most potent **inhibitor** of [^{11}C]cyano-dizocilpine binding was (+)-dizocilpine, followed by cyano-dizocilpine and (−)-dizocilpine with half-inhibition concentrations (IC_{50}) of 37.3 ± 7.1, 65.8 ± 8.8, and 445 ±

Figure 4-2. Inhibition of [^{11}C]cyano-dizocilpine binding by unlabeled cyano-dizocilpine (filled circles), (+)-dizocilpine (open circles), (-)-dizocilpine (open triangles), and ketamine (filled triangles). P_2-fraction of rat forebrain homogenate was incubated with 10 nM [^{11}C]cyano-dizocilpine for 40 min in the presence of various concentrations of displacing compounds, 1 mM L-glutamate, and 30 µM glycine. The data are mean values ± SEM of three experiments, each carried out in duplicate.

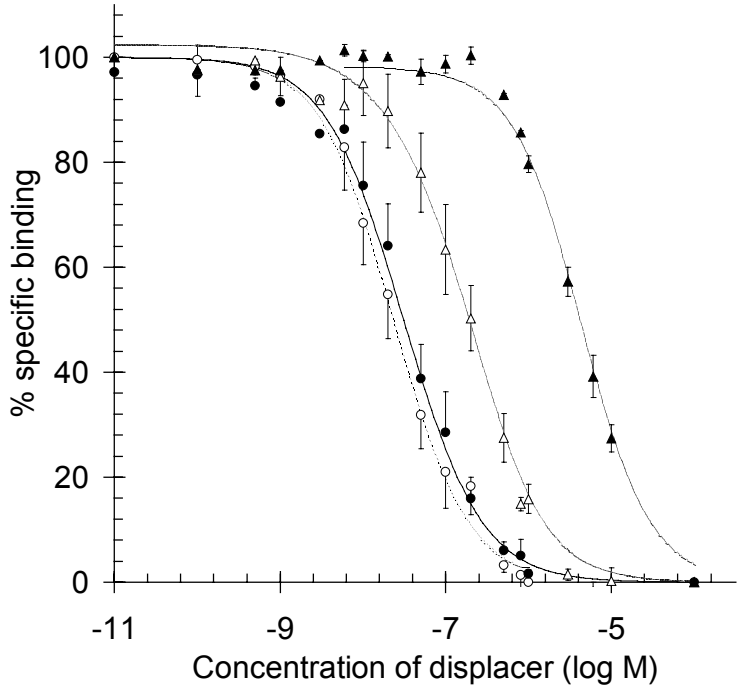

74.7 nM, respectively (**Figure 4-2**). Ketamine was about 100 times less potent, with an IC_{50} of 3.91 ± 0.3 µM. The highest distribution of specific binding of [^{11}C]cyano-dizocilpine in rat brain **frozen-section autoradiography** was observed predominantly in telencephalic regions, i.e., in the hippocampus and cerebral cortex. A moderate density of binding sites was found in the striatum and thalamus and a low density in the cerebellum, midbrain, pons, and brainstem. This pattern corresponds to that found in the autoradiographic studies on the distribution of [^{3}H]dizocilpine[17,217] and L-[^{3}H]glutamate binding sites[175] in the rat brain. At a 10 nM concentration, the specifically bound fraction amounted on average to 78 ± 4.5 % of the total binding.

In vivo **PET** with [^{11}C]cyano-dizocilpine showed a considerably high brain uptake. Intravenous pretreatment with (+)-dizocilpine, 0.1 mg/kg, or with ketamine, 2.5 mg/kg of body weight, prior to the bolus injection of [^{11}C]cyano-dizocilpine did not cause any change in the radiotracer retention kinetics. Obviously, a large proportion of the [^{11}C]cyano-dizocilpine that entered the brain was not associated with the specific recognition site during the investigation period. In mouse brain after intravenous injection of [^{3}H]dizocilpine, the maximum levels in brain tissue were reached within 10 min; but the specifically bound fraction constituted barely 4 % of the total brain radioactivity.[207] A rapid metabolic degradation of [^{11}C]cyano-dizocilpine, as well as the contribution of labeled metabolites during the 60-min study period, is very unlikely to have occured; since the maximal plasma levels of unmetabolized dizocilpine in monkeys was observed at 2 hrs after administration, and the major metabolites should not enter the CNS.[111] [^{11}C]Cyano-dizocilpine showed high uptake in the kidney cortex, heart muscle, liver, and adrenals, which may have been modified by displacing agents such that the whole-body balance was shifted, resulting in increased availability of the radiotracer in the brain in the displaced condition. This would explain the increased uptake of [^{11}C]cyano-dizocilpine under displacement conditions. The activation of NMDA receptors could be minimized further by isoflurane (the general anesthetic used in the present study) diminishing the chances of visualizing the active receptors. It has been shown that isoflurane antagonizes noncompetitively the concentration-dependent depolarizing effect of NMDA in preparations of mouse cortical wedges,[26] probably due to an interaction between the anesthetic drug and the allosteric glycine site or other multiple

allosteric sites that influence the activation of the ion channel.[152,153] Nevertheless, it has been shown that the pathological activation of the NMDA receptor causes an elevation in the uptake of labeled dizocilpine derivatives. However, this occurs at the late time points after tracer administration, showing the suitability of the use of these tracers under *in vivo* conditions.[160,198,254] Previously, a low specificity of racemic dizocilpine was considered as a drawback for visualizing the activation of NMDA receptors with that compound.[15] An active stereoisomer was used in the present study. Plotting the average peak uptake of [^{11}C]cyano-dizocilpine or average value from the last three time frames against rCBF values from the preceding $C^{15}O_2$ study for a selection of ROIs showed a rCBF-dependence of [^{11}C]cyano-dizocilpine uptake. Distribution of values from different [^{11}C]cyano-dizocilpine studies did not differ with 95 % confidence. The rCBF dependence might explain also the variability in baseline uptake of [^{11}C]cyano-dizocilpine. Perhaps the dominating rCBF component would dissipate after a longer observation time.

4.2 Applying *in vitro* tracer studies in neurotrauma

A wide range of tracers available in modern PET centres in connection with clinics, calls for methods to explore the properties of the tracers in disease models that correlate with human pathology as closely as possible before maximally meaningful projects can be planned in patients.

Glucose vs. fluorodeoxyglucose

Table 4-3 summarizes the uptake of FDG and [^{99m}Tc]HMPAO, in the *ex vivo* frozen section autoradiography standardized to the injected volume of tracer and body weight of the rat. In the present study, the **regional cerebral FDG uptake acutely after FPI** was significantly increased in the cortex ipsilateral to the site of injury as compared with that in the corresponding ROI in sham operated-animals or with that in the contralateral side. Also, it was significantly increased in the ipsilateral hippocampus, as compared with the contralateral hippocampus at the same level. By intention, the metabolic rate of glucose was not calculated, and the uptake of FDG was quantified by normalizing the values from autoradiograms to the injected amount of radioactivity and to the body weight of the animal.

Table 4-3. Uptake of FDG and ^{99m}Tc-labeled HMPAO in rat brain after parasagittal fluid-percussion injury; I-ipsilateral, C-contralateral to the injury. Uptake is standardized to the injected volume of tracer and body weight of the animal. Values are mean ± standard deviation. For comparison of the uptake to the corresponding ROI in sham-operated animals, the t test for independent samples was used; and P values are expressed as * P < 0.05, ** P < 0.01, *** P < 0.001. For comparison to contralateral side in the same animal, the paired t test was used; and results are marked † P < 0.05, †† P < 0.01, ††† P < 0.001.

Cerebral FDG uptake per injected volume and body weight

		Frontoparietal cortex		Hippocampus	
Time after trauma		Sham	Injured	Sham	Injured
42 min	I	47 ± 3	60 ± 5 **††	45 ± 4	52 ± 7 †
	C	49 ± 5	46 ± 8	44 ± 5	46 ± 5
	n	5	5	5	5
12 hrs	I	76 ± 16	32 ± 4 ***††	58 ± 15	40 ± 5 *††
	C	76 ± 18	69 ± 8	58 ± 17	49 ± 7
	n	4	5	4	5

[^{11}C]HMPAO uptake per injected volume and body weight

		Frontoparietal cortex		Hippocampus	
		Sham	Injured	Sham	Injured
42 min	I	25 ± 2	21 ± 3 †	25 ± 2	24 ± 5
	C	26 ± 2	27 ± 7	25 ± 2	25 ± 5
	n	5	6	5	6
12 hrs	I	47 ± 2	17 ± 1 ***†	37 ± 2	21 ± 6 **††
	C	47 ± 2	29 ± 6 ***	37 ± 2	24 ± 5 **
	n	5	4	5	4

An accepted explanation for the immediate reversible increase in posttraumatic LCMRG is that the cells have to meet an increased energy demand in their efforts to restore normal ionic balance disrupted by ionic shifts through transmitter-gated ion channels.[191,192,130,131,129] Increased rates of oxidative phosphorylation and mitochondrial synthesis of ATP have been detected after moderate lateral FPI in rats.[253] Although a constant level of ATP was found, the ADP and AMP levels were increased during the first four hours after the FPI, providing a stimulus for increased glycolysis for maintenance of a metabolic steady state. Although some acidosis and a transient increase in lactate concentration have been observed after TBI,[131] there are other studies[253,161,117,4] showing that moderate FPI does not result in uncontrolled glycolysis and lactic acidosis. It seems possible that the increase in energy demand is well covered by uncompromised oxidative metabolism paralleled by independently stimulated glycolysis. With regard to substrate supply, there are studies showing increased oxygen consumption immediately after TBI.[189,145] The key point in glycolysis is the essentially irreversible phosphorylation of glucose by hexokinase.[8] As Sokoloff *et al*.[233] (1977) recognized, DG exhibits a lower affinity for hexokinase than glucose in the normal brain, where most of the neural hexokinase exists in soluble form in the cytosol.[199] Due to the difference in kinetics between DG and glucose, the operational equation for calculating LCMRG by the DG method from autoradiographic images uses a lumped constant (LC) to correct for the lower rate of DG phosphorylation as compared with the rate for glucose. The LC has been measured to be around 0.5 with DG[233] and around 0.6 with FDG.[143] Conditions in which energy utilization exceeds the glucose supply shift the solubilization equilibrium of hexokinase to the bound mitochondria form, which is more active and has higher affinity for the substrate,[250] as a fine tuning of the activity of the initial enzyme in glycolysis in response to changes in the cellular environment. The LC[187,77] as well as the mitochondrial binding of cortical hexokinase[76] are both increased during ischemia. Using the DG method with a uniform LC throughout all brain structures would, in such case, cause an overestimation of LCMRG in "hot spots" of the autoradiogram. In the transplantable rat glioma, more than 2-fold higher LC has been shown in comparison with the constant for normal brain tissue,[127,236] and this is in agreement with the view that the mitochondrial-bound form of hexokinase plays a key role in the high aerobic glycolysis of tumor cells.[25]

Deoxyglucose has a higher affinity for endothelial transport than glucose.[71] A significant correlation exists in the adult SpD rat brain between endothelial transporter densities and local cerebral glucose utilization measured by the DG method.[270] Nearly half of the endothelial (blood-brain barrier, BBB) glucose transporter protein (Glut1) is normally contained within the cytoplasmic space, which provides a mechanism for rapid up-regulation of the transporter on the luminal membrane of the capillary endothelial wall,[56] as was shown to occur in human seizures.[30] Later studies by Cornford *et al*.[31] (1996) demonstrated an increased activity of Glut1 in human brain areas of severe injury with a concomitant compromised function of the BBB and suggested that the regulation of the membrane transporter activity was controlled ultimately by individual brain capillary cells.

Table 4-4 summarizes the SUVs of FDG and [1-^{14}C]glucose from **double-tracer studies** performed at **7 or 17 min after trauma** (10 or 20 min after injection of the tracers, respectively). The SUV of FDG at the trauma site cortex was significantly higher than that in the corresponding region on the contralateral side. In the hippocampi a significantly higher SUV of FDG appeared only at the later time point (17 min from TBI, 20 min after the injection). The average ipsilateral to contralateral ratios of SUVs of FDG in the cortex were 1.3 and 1.5, and those in the hippocampi, 1.1 and 1.2 (10 and 20 min after tracer

injection, respectively); whereas the ipsilateral to contralateral ratios of [1-^{14}C]glucose SUVs were 1.0 ± 0.1 on the average.

The present study failed to confirm an increased focal uptake of [1-^{14}C]glucose in the frontoparietal cortex and in the hippocampus immediately after moderate FPI. The differently changed kinetics of glucose and FDG for BBB transport and subsequent phosphorylation might be the cause behind it; particularly, the increased affinity of FDG in comparison to glucose in either of the above described processes. The rationale of measuring glucose turnover with labeled glucose lies in the fact that the substrate of interest and tracer are identical. Metabolic rates of glucose can be measured with ^{14}C-labeled glucose despite the rather rapid loss of the radiolabel as $^{14}CO_2$ and [^{14}C]lactate. In fact, the ability to complete measurements in a short time period can be a significant benefit. It could be of advantage to use ^{11}C-labeled glucose and PET[16] to visualize the glucose utilization in such conditions as acute experimental TBI, where the rate of glucose turnover is dynamic and the conditions contained within the lumped constant might vary from what are currently known. Previously, nearly identical values for LCMRG were obtained from [6-^{14}C]glucose data from an experiment of 5-min duration and from FDG data from one of 45-min duration in normal rats.[92] The loss of ^{14}C via $^{14}CO_2$ in the case of [2-^{14}C]glucose has been estimated to be 8% at 10 min.[90] On the other hand, at 6 and 12 min postinjection of [6-^{14}C]glucose, 10% and 18%, respectively, of the radiolabel was lost as $^{14}CO_2$. In the case of [1-^{14}C]glucose additional loss due to small activity of the nonenergy-yielding pentose phosphate pathway should be expected.[142] The pentose shunt that removes 1-carbon has a low activity in the normal brain;[91] but it might be activated by oxidative stress demands on the glutathione pathway, causing a larger fraction of glucose to enter the pentose phosphate pathway.[10] The underestimation of LCMRG using position-6 labeled [^{14}C]glucose was shown to be metabolic rate dependent.[142] Hawkins *et al.*[93] (1994) proposed a 7 to 14 % underestimation of LCMRG at rates from 60 to 90 μmol/100 g/min with [6-^{14}C]glucose and a 10-min experimental time period as used in the present study. About 60 and 90 μmol/100 g/min were the highest acute increases in LCMRG at the trauma-site cortex in the studies by Ginsberg *et al.*[70] (1997) and Yoshino *et al.*[268] (1991), respectively. Much lower maximum values can be imagined in the present study because of the use of pentobarbital anesthesia,

Table 4-4. Standardized uptake of FDG and D-[1-^{14}C]-glucose in brain tissue pieces. Tracers were injected 3 min prior to TBI. The animals were decapitated 10 or 20 min after the injection of the tracer. I-ipsilateral, C-contralateral. A. 7 and 17 min after brain trauma, B. 11 hrs and 45 min after TBI. Values are means ± StdDev. The paired t test was performed for statistical significance of the diference between IL and CL, * indicates P value smaller than 0.05

	Time after injection of tracer					
	10 min			20 min		
A, acutely after trauma (n=5)	I	C	I / C	I	C	I / C
Cortex, FDG	4.2 ± 1.2 *	3.1 ± 0.6	1.3 ± 0.2	4.7 ± 0.3 *	3.2 ± 0.4	1.5 ± 0.1
Cortex, [^{14}C]Glucose	4.2 ± 1.8	4.2 ± 1.7	1.0 ± 0.1 *	4.7 ± 1.2	4.8 ± 1.7	1.0 ± 0.1 *
Hippocampus, FDG	3.5 ± 0.9	3.3 ± 0.8	1.1 ± 0.1	4.1 ± 0.3 *	3.4 ± 0.1	1.2 ± 0.1
Hippocampus, [^{14}C]Glucose	3.6 ± 1.5	3.5 ± 1.5	1.0 ± 0.1	4.3 ± 1.3	3.9 ± 0.8	1.1 ± 0.1
B, 12 hrs after trauma (n=3)						
Cortex, FDG	2.3 ± 0.4 *	3.9 ± 0.5	0.6 ± 0.11			
Cortex, [^{14}C]Glucose	3.7 ± 0.4 *	5.3 ± 0.8	0.7 ± 0.04			
Hippocampus, FDG	2.1 ± 0.2 *	2.7 ± 0.4	0.8 ± 0.05			
Hippocampus, [^{14}C]Glucose	3.1 ± 0.3 *	3.9 ± 0.4	0.8 ± 0.04			

whereas enflurane and halothane, respectively, were used with a mixture of nitrous oxide and oxygen in the two studies mentioned above. In the case of a substantial increase in energy demand, the additional ATP production would be covered by glycolysis,[62] resulting in lactate production. If a significant quantity of lactate would have been produced from [1-^{14}C]glucose during the first 15 min after FPI, as shown by Kawamata *et al.*[131] (1995), then the risk of loss of the radiolabel via lactate exit from the brain would be minimal. Measurement of the tissue radioactivity was performed before the lactate concentrations would be expected to return to baseline levels. In such a situation, the measured [1-^{14}C]glucose metabolites reflect the oxidative component of metabolism contaminated by labeled lactate. Moreover, only a negligible amount of the [6-^{14}C]glucose that was taken up by the brain during a 10-min period following the injection was then released to the blood as [^{14}C]lactate in normal adult rats or in rats with seizures.[93]

At 12 hrs after the trauma, the **FDG** uptake was decreased significantly, both in the trauma-site cortex and in the underlying hippocampus. At the trauma-site frontoparietal cortex, a decrease of 50% was seen in frozen-section autoradiography. This finding corresponds well with previous results obtained by the DG method.[268,43] The metabolic depression was demonstrated with **[1-^{14}C]glucose** as well in the frontoparietal cortex and hippocampus ipsilateral to the site of the injury as compared with the uptake in the corresponding contralateral regions, at 10 min after the injection of the tracers. The acute uptake of FDG in the frontoparietal cortex of sham-operated animals was lower, being, on the average, 63% of the corresponding uptake value at 12 hrs after the sham-operation. That the controls showed an average of 37% lower uptake of FDG acutely after the sham-operation as compared with that at 12 hrs after the sham-operation might be explained by the inhibitory effect of pentobarbital on oxidative metabolism[27] and the solubilization of mitochondria-bound hexokinase,[137] which might lower the affinity of FDG for hexokinase.

Regional cerebral blood flow (rCBF), as indicated by the trapping of [^{99m}Tc]HMPAO, was decreased at the trauma site cortex **by 42 min** after FPI in comparison with that on the contralateral side, but not when compared wth the corresponding ROI in sham-operated animals. The blood flow in the hippocampi did not appear to change acutely after the injury (**Table 4-3**). **At 12 hrs** after FPI, the rCBF was bilaterally decreased in the injured animals in all investigated regions in comparison with that in the sham-operated animals. Moreover, the trauma-site cortex and underlying hippocampus exhibited significantly lower rCBF than their contralateral counterparts. The acute rCBF in the frontoparietal cortex of sham-operated animals was on the average, 53% of the rCBF at 12 hrs after the sham operation.

Severely disturbed blood flow could be detected with [^{99m}Tc]HMPAO autoradiography at 12 hrs from FPI in the present study. Although absolute values were not measured, a blood flow above the ischemic threshold could be expected after moderate FPI.[264] As in the case of FDG uptake, the regional cerebral blood flow (rCBF) was also estimated as tracer uptake normalized to total administered radioactivity and body weight of the animal. Identical flow distribution was shown in the double-tracer autoradiographic images of [^{99m}Tc]HMPAO and [^{125}I]iodoamphetamine (IMP) in the same animals.[154] The relationship between [^{99m}Tc]HMPAO uptake and rCBF measured with [^{14}C]iodoantipyrine ([^{14}C]IAP) was linear at lower rCBF levels (up to 200 ml/100 g/min), and an excellent correlation followed thereafter up to 700 ml/100 g/min.[52] Yamakami and McIntosh[264] (1991) showed an average of 45% decrease bilaterally in rCBF 30 min after moderate FPI in isoflurane-anesthetized rats, with only a 10% difference between ipsi- and contralateral sides, with the rCBF in the contralateral side being higher. The ipsilateral rCBF was shown

to remain decreased during the first days after lateral FPI.[264,70] Pentobarbital, which was used in the present study, was shown to cause a 40-50% decrease in rCBF in normal rats.[155,243] An already low rCBF could then explain why only about 20% additional decrease in [^{99m}Tc]HMPAO uptake was observed acutely at the trauma-site cortex. Platelet accumulation and edema formation could serve as probable causes of this perfusion deficit.

NMDA -, mACh -, and $GABA_A$ receptors after traumatic brain injury

In **[^{11}C]cyano-dizocilpine autoradiography**, the general binding pattern showed the highest specific binding in the hippocampus and cerebral cortex. A moderate density of binding sites appeared in the striatum and thalamus and a low density in the midbrain, pons, and brainstem. Two hours after FPI, there was a tendency for decreased binding site number (B_{max}) and affinity; and the binding potential (BP= B_{max}/K_D, **Table 4-5**) showed a significant decrease bilaterally for the frontoparietal cortex and hippocampus in comparison with that of the sham-operated animals. At 12 hrs from trauma the affinity (**Figure 4-3**) was bilaterally decreased in the cortex and hippocampus as compared with that of the sham-operated animals. Additionally, a significant decrease in B_{max} (**Figure 4-4**) was seen at the trauma-site cortex, which was 60% of the value for the sham-operated animals or for the contralateral side. A total (in frontoparietal cortex and hippocampi, bilaterally) decrease in BP of [^{11}C]cyano-dizocilpine was seen at 12

Figure 4-3. Dissociation constant (K_D) of [^{11}C]cyano-dizocilpine, 4-N-[^{11}C]methylpiperidylbenzilate, and [^{11}C]flumazenil in rat brain after moderate lateral fluid-percussion injury (FPI). Values are means ± SEM. For comparison of the binding constants with the corresponding ROI in sham-operated animals, the t test for independent samples was used; and P values are expressed as *P<0.05, **P<0.01, ***P<0.001. For comparison with the contralateral side, the paired t test was used; and results are marked †P<0.05, ††P<0.01, †††P<0.001. "a" Indicates significant difference (P<0.005) between sham-operated animals at 12 and 2 hrs after FPI.

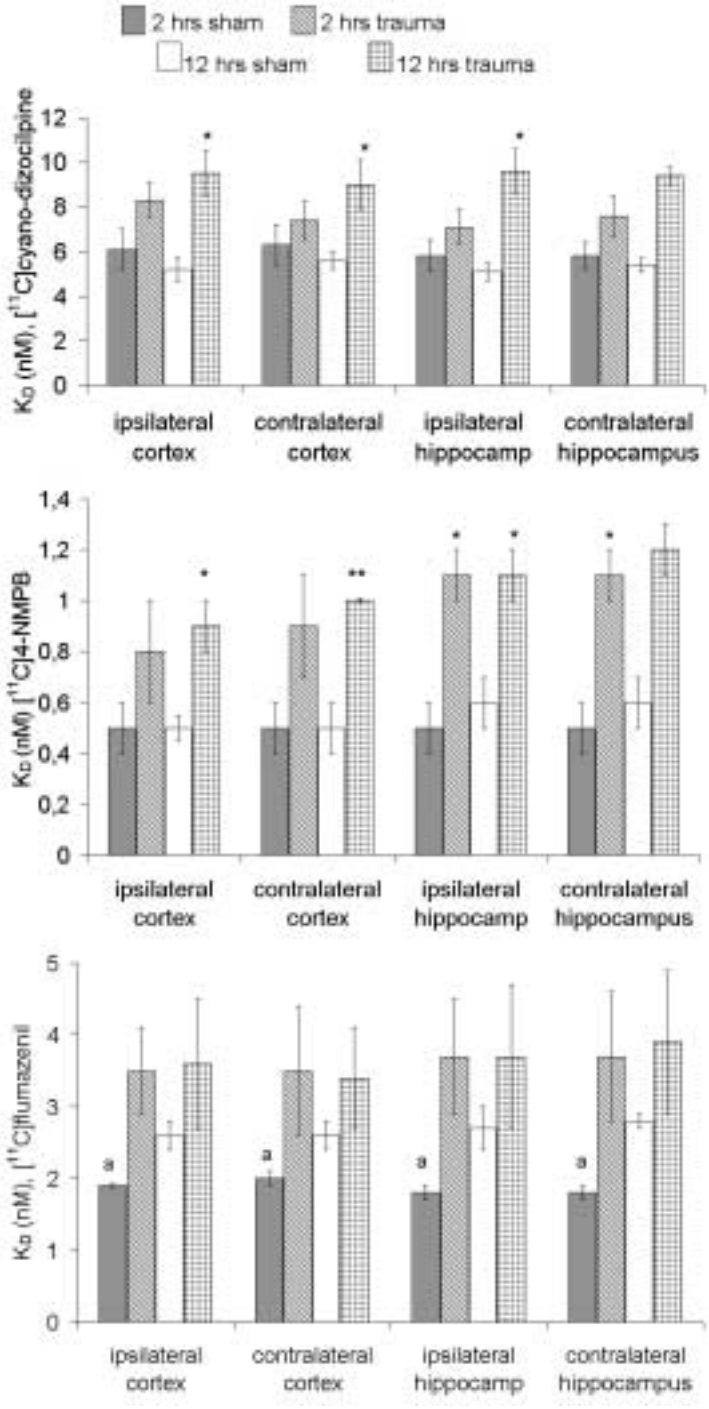

Figure 4-4. Maximum number of binding sites (B_{max}) of [^{11}C]cyano-dizocilpine, 4-N-[^{11}C]methylpiperidylbenzilate, and [^{11}C]flumazenil in rat brain after moderate lateral fluid-percussion injury (FPI). Values are means ± SEM. For comparison of the binding constants with the corresponding ROI in sham-operated animals, the t test for independent samples was used; and P values are expressed as *P<0.05, **P<0.01, ***P<0.001. For comparison with the contralateral side, the paired t test was used; and results are marked †P<0.05, ††P<0.01, †††P<0.001.

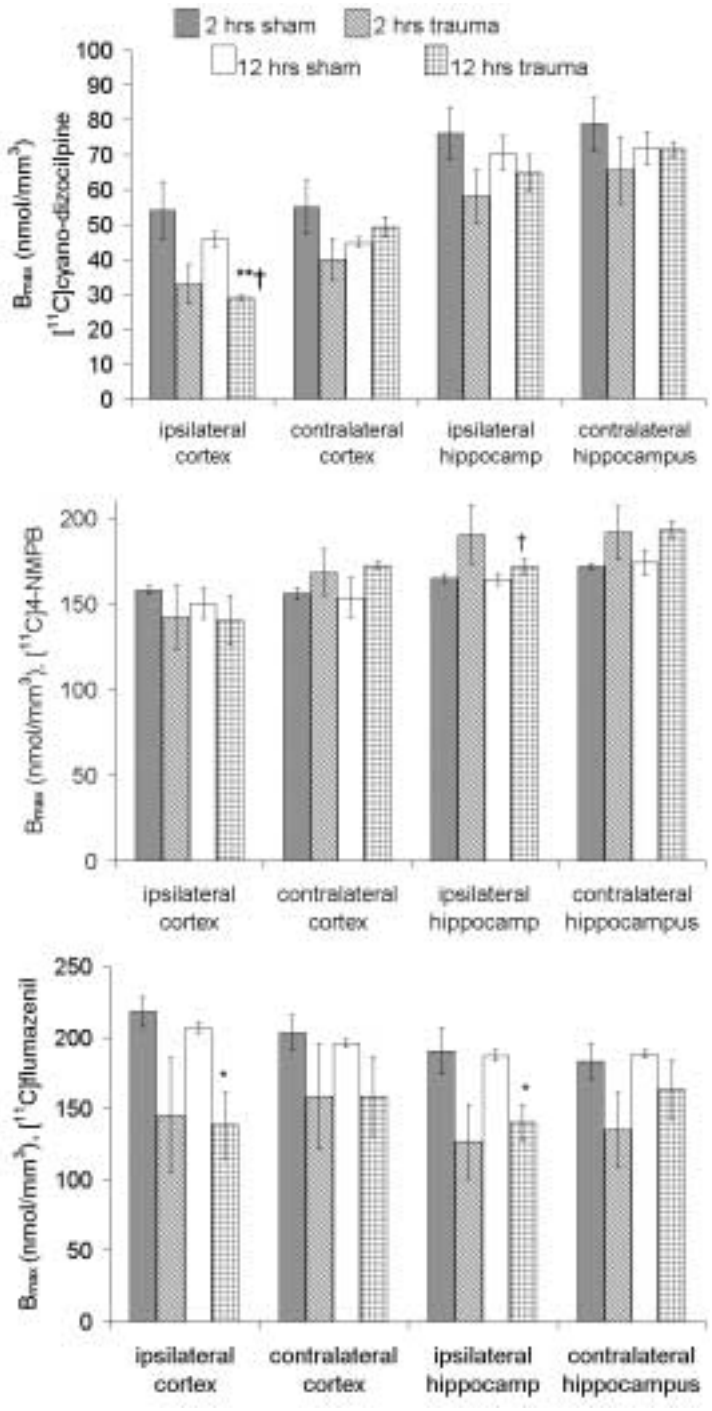

hrs, and it was significantly more prominent in the ipsilateral cortex and hippocampus. Miller and co-workers (1990)[173] showed lowered binding of [^{3}H]glutamate to NMDA receptors at 3 and 24 hrs after TBI in cortex and hippocampus. A 5-min time point investigated by them showed statistically non-significant changes in [^{3}H]glutamate binding in all investigated regions excluding the inner cortex, where it was significantly lower. The preincubation procedure used for removing endogenous ligands in their autoradiography was omitted by the use of [^{11}C]cyano-dizocilpine in the present work. Regardless of that, no increased affinity was seen as it would be expected from *in vitro* studies with tracers that bind to a site inside the ion-channels of NMDA receptors.[61,III] It is probable that overactivation of NMDA receptors in experimental TBI lasts only a short time after the impact. Increased extracellular glutamate concentrations, after experimental TBI, were detected during the first minutes[109,191] to an hour[246,72] after TBI. There are other studies supporting the suggestion that the excessive excitation of NMDA and also of mACh receptors is brief (less than 15 min) and that the antagonism of particular receptor systems after that time has no positive effect on the recovery of cognitive function following TBI in the rat.[84]

The highest **[^{11}C]4-NMPB** binding density was found in the striatum, followed by hippocampus and cerebral cortex; and the density was much lower in the other structures of the brain. At 2 hrs after FPI there was a bilaterally significant 2-fold decrease in

affinity in the hippocampus. There were no significant changes in binding site number in the traumatized rats in comparison with the corresponding investigated regions in the sham-operated animals. Only a significantly lower value for B_{max} was found in the hippocampus underlying the trauma site in comparison with the value for the contralateral corresponding region. At 12 hrs from FPI the affinity of [^{11}C]4-NMPB for mACh receptors was decreased in all investigated regions, and B_{max} was significantly decreased in the trauma-side hippocampus as compared with that in the contralateral side. The BP was significantly decreased at 2 hrs from FPI for the trauma-side hippocampus; and at 12 hrs from FPI, it was decreased for all investigated regions excluding the contralateral cortex. Similar to the findings of previous studies,[150] a decreased affinity of antagonist for mACh receptors was seen in the present study. An early anticholinergic treatment was shown to attenuate motor deficits,[149] and to improve impaired cognitive function[205] following FPI in rats. At a longer time (15 days) after TBI, a significant upregulation of binding sites for [^{3}H]QNB was demonstrated;[123] and long-lasting changes in the function of the central cholinergic system after TBI in rats was shown.[75] The initial decrease in affinity of mACh receptor antagonists for their binding sites may reflect the inactivation of cholinergic receptors in response to massive acetylcholine release[74] immediately after the FPI. The prominent decrease in BP of [^{11}C]cyano-dizocilpine and [^{11}C]4-NMPB including the bilateral decrease in the affinity of these tracers reflects the damage to the NMDA and mACh receptor systems due to FPI.

The highest density of **[^{11}C]flumazenil** binding sites in investigated rat forebrains was noted in the cerebral cortex, followed by hippocampus and thalamic nuclei and then the rest of the regions. [^{11}C]Flumazenil exhibited a statistically significant increase in affinity for its binding site due to the pentobarbital anesthesia, as shown by comparing the binding in anesthetized sham animals at 2 hrs after the sham operation to the binding in conscious sham-operated animals at 12 hrs after the operation (significance $p<0.05$, labeled by "a" in **Figure 4-3**). This contributed to the significant increase in BP in acute sham-operated animals. Such an acute, reversible, and dose-dependent effect of barbiturates on benzodiazepine binding was demonstrated in earlier studies *in vivo*.[172] Acutely after FPI the tendency toward decreases in affinity and binding site number was obvious, this forming the basis for the significantly decreased BP of the trauma-site cortex and underlying hippocampus. At 12 hrs after FPI, the number of binding sites was significantly decreased in the trauma-site cortex and in the underlying hippocampus. At that time point the BP was significantly decreased only for the trauma-site cortex. The BP of other investigated tracers at 12 hrs after FPI was decreased in all investigated regions (excluding the contralateral cortex with [^{11}C]4-NMPB). This finding demonstrates the potential capability of [^{11}C]flumazenil to selectively depict the regions with neuronal damage, leading to visible loss of thionin-stained neurons, which begins by 12 hrs after moderate-level FPI.[102] [^{11}C]Flumazenil was shown to demonstrate the extent of neuronal damage and predict the possible recovery after focal ischemia in animals[223,97] and also in patients with acute stroke[98,99] or in an acute vegetative state.[214] The $GABA_A$ ergic neurotransmission, which is a major counterbalance to the excitotoxic mechanisms *in vivo*, has only minimally been investigated in experimental TBI. A reversible increase in the extracellular GABA concentration was shown by microdialysis in concussive brain injury in rats.[191] Recently, improved effects on mortality and cognitive outcome were observed in rats subjected to moderate level FPI after pretreatment with diazepam.[193] Postinjury treatment did not enhance the survival but induced significantly better recovery of cognitive function.

Table 4-5. Binding potential: B_{max}/K_D. Values are means ± SEM. For comparison of the binding potential between traumatized and sham-operated animals, the t test for independent samples was used; and P values are expressed as *P<0.05, **P<0.01, ***P<0.001. For comparison with the contralateral side in the same animal, the paired t test was used; and results are marked †P<0.05, ††P<0.01, †††P<0.001. For comparing values from sham-operated animals at 12 hrs with those at 2 hrs, the t test for independent samples was used; and P values are expressed as $^{a}P < 0.05$.

	Binding potential			
	Cortex		Hippocampus	
	Trauma site	Contralateral	Trauma site	Contralateral
[^{11}C]dizocilpine				
2 hrs, sham	8.8 ± 0.4	8.8 ± 0.4	13.4 ± 1.1	13.6 ± 0.9
2 hrs, trauma	3.9 ± 0.4***	5.4 ± 0.2**	8.1 ± 0.2**	8.6 ± 0.2**
12 hrs, sham	8.9 ± 0.4	8.1 ± 0.3	14.0 ± 0.4	13.3 ± 0.2
12 hrs, trauma	3.1 ± 0.5***†	5.6 ± 0.5*	6.9 ± 0.6***†	7.7 ± 0.5***
[^{11}C]4-N-methylpiperidylbenzilate				
2 hrs, sham	347.0 ± 56.0	316.3 ± 59.2	327.0 ± 52.4	354.9 ± 90.4
2 hrs, trauma	196.0 ± 50.8	193.6 ± 31.3	175.5 ± 10.3*	182.8 ± 18.7
12 hrs, sham	311.8 ± 33.6	318.9 ± 61.6	309.5 ± 78.6	290.9 ± 34.1
12 hrs, trauma	159.0 ± 6.1*	174.5 ± 2.3	170.1 ± 16.6*	167.6 ± 5.0*
[^{11}C]flumazenil				
2 hrs, sham	117.0 ± 7.2 [a]	104.3 ± 7.8 [a]	103.7 ± 11.0	102.9 ± 9.9 [a]
2 hrs, trauma	45.8 ± 17.7*	55.8 ± 25.0	41.5 ± 18.0*	47.0 ± 22.7
12 hrs, sham	81.0 ± 6.3	75.0 ± 6.0	71.8 ± 8.2	67.1 ± 4.5
12 hrs, trauma	42.5 ± 11.1*	50.5 ± 13.8	43.5 ± 12.4	47.8 ± 14.3

5. SUMMARY

Positron-emitting radiotracer substances can with benefit be used for *in vitro* assessment of receptor kinetic parameters. Conventional assay methods can be applied with some minor modifications to account for factors such as a short half-life and emission of β^+-particles. Some of the properties of positron-emitting radiotracers create extra advantages for *in vitro* work; for example, potentially super high specific activity, rapidity of experiments, and the potential to readily apply the methods *in vivo*. The SP plate system is a very attractive measuring device with good physical performance for this type of work. For the application of PET tracers to autoradiography, different properties of the tracers, and the phosphor imaging measurement system must be considered. Quantitative autoradiography can be performed with short-lived PET tracers, but, it is necessary to consider that the time to reach equilibrium is dependent on the section thickness. The use of thicker sections gives a better signal and thus better resolved images but, perhaps at the expense of deteriorated quantification. Because of the short half-life of the label, the equilibrium conditions might not be met. The SP plate is an ideal tool for generation of ^{11}C images because of its high sensitivity and linear response over a wide concentration range.

[^{11}C](+)3- and [^{11}C]4-NMPB are non-selective with respect to subtypes of muscarinic ACh receptors. Depending on the experimental conditions in frozen-section autoradiography, different subtypes may be accentuated. Either [^{11}C](+)3- or [^{11}C]4-NMPB is suitable for PET studies of mACh receptors. Differential labeling of mACh receptors cannot, however, be anticipated. A newly developed labeled analogue of dizocilpine, [^{11}C]cyano-dizocilpine binds specifically to the NMDA type of glutamate receptors *in vitro*. Under the tested conditions, a specific binding of [^{11}C]cyano-dizocilpine *in vivo* could, however, not be visualized by PET, due probably to the high fraction of nonspecific binding. The present work suggests that future attempts at visualizing the activity of the NMDA-receptor-channel complex *in vivo* by PET should utilize unanesthetized research animals. Synthesis of tracers with lower lipophilicity but with high affinity for the receptor retained should also be tried.

The increased uptake of [^{18}F]fluorodeoxyglucose after experimental brain trauma could not be confirmed with [1-^{14}C]glucose. The lack of increase in [1-^{14}C]glucose uptake in contrast to the increased FDG uptake immediately after moderate FPI could be explained by the increased postraumatic affinity of FDG for the endothelial glucose transporter proteins and/or for hexokinase. Postraumatic differences in the kinetics of FDG entry to the brain and phosphorylation can cause erroneous results of local cerebral glucose utilization as measured with FDG (or deoxyglucose), when a uniform and fixed lumped constant derived from normal subjects is used. The fulfillment of the assumptions underlying the deoxyglucose method (incl. lumped constant) is a necessary precaution when the deoxyglucose method is used in pathologic conditions, as has been suggested already by the authors of the method. The present work demonstrated that a moderate level of lateral FPI caused general as well as localized changes in neurotransmitter receptor systems that could be measured by *in vitro* quantitative autoradiography. Diffusely spread decreased affinity of NMDA - and mACh receptor ligands is an indicator of not only local disturbed neurotransmission as could be expected from locally increased glucose turnover as measured by FDG primarily at the trauma site, but of widely dissipated disturbance of neurotransmission. Localized changes in [^{11}C]flumazenil binding to $GABA_A$ receptors may indicate the potential capability of [^{11}C]flumazenil to selectively depict the regions with neuronal damage that leads to loss of neurons.

6. ACKNOWLEDGMENTS

This study was carried out at the preclinical laboratory of Uppsala University PET Centre in collaboration with the Unit of Pharmacology, Department of Neuroscience, Faculty of Medicine, Uppsala University.

I am grateful for the help I have received from colleagues and friends in preparing this thesis. In particular:

Assoc. Prof. Mats Bergström, Profs. **Yasuyoshi Watanabe**, **Bengt Långström**, and **Lars Oreland**, for being a nice team of supervisors, for providing their facilities and innovative ideas, and for sharing their knowledge, experience, and support;

Drs. Yvonne Andersson, **Karl-Johan Fast**, **Matthias Ögren**, **Gunilla Jacobson**, **Gunnar Antoni**, and **Margareta Björkman**, and **Misses Anna Bergman** and **Pernilla Sjöberg**, for their excellent tracer labeling all these years, for not forgetting me waiting for a tracer, and for a second chance in the event of technical problems;

Dr. Niklas Marklund, for teaching me the trauma models and for sharing his never failing optimism, and **Assoc. Prof. Urban Höglund**, for sharing his scientific knowledge;

Mrs. Elisabeth Petterman-Bergström and **Dr. Feng Wu** for assistance and help in the lab, and **Dr. Li Lu** for teaching me the skill of hitting a rat tail vein with the injection needle and for her nature of not saying "No" when I asked for help;

Messrs. Harald Schneider and **Tomas Nyberg**, for taking excellent care of the computers; Nurses **Karin Lidström**, **Lars Lindsjö**, **Eva-Lise Lundberg**, **Rita Öhrstedt**, and **Mimmi Lidholm**, for taking excellent care of the experimental monkeys and PET cameras, and for creating a relaxed working atmosphere; **Mr. Leif Ormegard**, for his exquisite handling and care of the experimental monkeys and for being the person who managed with friendly chats to open up my Swedish language;

Dr. Daniel Laryea, for revising the English in the thesis and for interesting and encouraging discussions.

My Japanese friends, **Drs. Kiyoshi Matsumura**, **Tetsuhito Murata**, **Hirotaka Onoe**, and **Kazuyuki Imamura**, for interesting discussions, help, advice, and kind hospitality;

Giussi and **Tom**, **Roberta** and **Björn**, for friendship and very valuable recreational times;

My friends in Tartu, for making me feel at home during my continuous medical education at Tartu University; and **Dr. Kai Saks** and **Prof. Helgi Silm**, former Assistant Deans at the Faculty of Medicine, Tartu University for supporting my individual study schedule during the research work at Uppsala University;

Dr. Wiebke Sihver, for having a direct and great impact on this work by placing her scientific knowledge and experience at my disposal whenever I asked for it, for pertinacious and kind support during those times I felt like changing "business", and for indirect impact via the numerous stimulating adventures we have shared together as a family, and above all, for her warmth and love.

Finally, I am also grateful to my children, **Gertu** and **Ragnar**, for being so sweet, for teaching me the art of waking up early during weekends, and for giving me yet another chance to visit amusement parks!

This work was financially supported by the Subfemtomole Biorecognition Project, Uppsala University PET Centre, and Japan Science and Technology Corporation.

REFERENCES

1. Abu-Judeh HH, Singh M, Masdeu JC, Abdel-Dayem HM (1998) Discordance between FDG uptake and technetium-99m-HMPAO brain perfusion in acute traumatic brain injury. *J Nucl Med* 39:1357-1359.
2. Alavi A, Fazekas F, Alves W, Rosen M, Lang TW, Zimmerman RA, Kushner M, Chawluk JB, Reivich M (1987) Positron emission tomography in the evaluation of head injury. *J Cereb Blood Flow Metab* 7:S646.
3. Alavi A, Newberg AB (1996) Metabolic consequences of acute brain trauma: is there a role for PET? *J Nucl Med* 37:1170-1172.
4. Andersen BJ, Marmarou A (1992) Post-traumatic selective stimulation of glycolysis. *Brain Res* 585:184-189.
5. Andersson Y, Tyrefors N, Sihver S, Onoe H, Watanabe Y, Tsukada H, Långström B (1998) Synthesis of a ^{11}C-labelled derivative of the N-methyl-D-aspartate receptor antagonist MK-801. *J Labelled Cpd Radiopharm* XLI:567-576.
6. Astrup J, Symon L, Branston NM, Lassen NA (1977) Cortical evoked potential and extracellular K+ and H+ at critical levels of brain ischemia. *Stroke* 8:51-57.
7. Auer R, Kalimo H, Olsson Y, Wieloch T (1985) The dentate gyrus in hypoglycemia: pathology implicating excitotoxin-mediated neuronal necrosis. *Acta Neuropathol (Berl)* 67:279-288.
8. BeltrandelRio H, Wilson JE (1992) Coordinated regulation of cerebral glycolytic and oxidative metabolism, mediated by mitochondrially bound hexokinase dependent on intramitochondrially generated ATP. *Arch Biochem Biophys 296:667-677*.
9. Benavides J, Peny B, Dubois A, Perrault G, Morel E, Zivkovic B and Scatton B (1988) In vivo interaction of zolpidem with central benzodiazepine (BZD) binding sites (as labeled by [^{3}H]Ro 15-1788) in the mouse brain. Preferential affinity of zolpidem for the ω1 (BZD1) subtype. *J Pharmacol and Exp Ther* 245:1033-1041.
10. Ben-Yoseph O, Boxer PA, Ross BD (1996) Assessment of the role of the glutathione and pentose phosphate pathways in the protection of primary cerebrocortical cultures from oxidative stress. *J Neurochem* 66:2329-2337.
11. Bergman C, Johansson KJ, Karlberg J, Larsson B, Lundquist H. Löfroth PO, Rosander K, Ryden BE, Stålnacke CG (1994) NaI(Tl)-Detectorer. In: *Strålskydd*. Edited by Jansson LT and Ryden BE), pp.100-102. Stockholm.
12. Bergsneider M, Hovda DA, Shalmon E, Kelly DF, Vespa PM, Martin NA, Phelps ME, McArthur DL, Caron MJ, Kraus JF, Becker DP (1997) Cerebral hyperglycolysis following severe traumatic brain injury in humans: a positron emission tomography study. *J Neurosurg* 86:241-251.
13. Bergström M, Westerberg G and Långström B (1997) ^{11}C-Harmine as a tracer for monoamine oxidase A (MAO-A): *in vitro* and *in vivo* studies. *Nucl Med Biol* 24:287-293.
14. Bergström M, Bonasera TA, Lu L, Bergström E, Backlin C, Juhlin C and Långström B (1998) In vitro and in vivo primate evaluation of carbon-11-etomidate and carbon-11-metomidate as potential tracers for PET imaging of the adrenal cortex and its tumors. *J Nucl Med* 39:982-989.
15. Blin J, Denis A, Yamaguchi T, Crouzel C, MacKenzie ET, Baron JC (1991) PET studies of [^{18}F]methyl-MK-801, a potential NMDA receptor complex radioligand. *Neurosci Lett* 121:183-186.
16. Blomqvist G, Stone-Elander S, Halldin C, Roland PE, Widen L, Lindqvist M, Swahn CG, Langstrom B, Wiesel FA (1990) Positron emission tomographic measurements of cerebral glucose utilization using [1-^{11}C]D-glucose. *J Cereb Blood Flow Metab* 10:467-483.
17. Bowery NG, Hudson AL (1986) The distribution of [^{3}H]-MK801 binding sites in rat brain determined by in vitro receptor autoradiography. *Br J Parmacol* 89: 775P.
18. Bowery NG, Hudson AL, Price GW (1987) $GABA_A$ and $GABA_B$ receptor site distribution in the rat central nervous system. *Neuroscience* 20:365-383.
19. Bowery NG, Wong EH, Hudson AL (1988) Quantitative autoradiography of [^{3}H]-MK-801 binding sites in mammalian brain. *Br J Pharmacol* 93:944-954.
20. Braestrup C and Squires RF (1977) Specific benzodiazepine receptors in rat brain characterized by high-affinity [^{3}H]diazepam. *Proc Natl Acad Sci USA* 74, 3805-3809.
21. Brown CL and Martin IL (1984) Kinetics of [^{3}H]Ro 15-1788 binding to membrane bound rat brain benzodiazepine receptors. *J Neurochem* 42:918-923.
22. Brown DR, Wyper DJ, Owens J, Patterson J, Kelly RC, Hunter R, McCulloch J (1997) ^{123}Iodo-MK-801: a spect agent for imaging the pattern and extent of glutamate (NMDA) receptor activation in Alzheimer's disease. *J Psychiatr Res* 31:605-619.
23. Buck A, Mulholland GK, Papadopoulos SM, Koeppe RA, Frey KA (1996) Kinetic evaluation of positron-emitting muscarinic receptor ligands employing direct intracarotid injection. *J Cereb Blood Flow Metab* 16: 1280-1287.
24. Bullock R, Zauner A, Myseros JS, Marmarou A, Woodward JJ, Young HF (1995) Evidence for prolonged release of excitatory amino acids in severe human head trauma. Relationship to clinical events. *Ann N Y*

Acad Sci 765:290-298.
25. Bustamante E, Morris HP, Pedersen PL (1981) Energy metabolism of tumor cells. Requirement for a form of hexokinase with a propensity for mitochondrial binding. *J Biol Chem* 256:8699-8704.
26. Carla V, Moroni F (1992) General anesthetics inhibit the responses induced by glutamate receptor agonists in the mouse cortex. *Neurosci Lett* 146: 21-24.
27. Carlsson C, Harp JR, Siesjö BK (1975) Metabolic changes in the cerebral cortex of the rat induced by intravenous pentothalsodium. *Acta Anaesthesiol Scand Suppl* 57:1-17.
28. Cheng Y, Prusoff WH (1973) Relationship between the inhibition constant (K1) and the concentration of inhibitor which causes 50 per cent inhibition (I50) of an enzymatic reaction. *Biochem Pharmacol* 22:3099-3108.
29. Collerton D (1986) Cholinergic function and intellectual decline in Alzheimer's disease. *Neuroscience* 19:1-28.
30. Cornford EM, Hyman S, Swartz BE (1994) The human brain GLUT1 glucose transporter: ultrastructural localization to the blood-brain barrier endothelia. *J Cereb Blood Flow Metab* 14:106-112.
31. Cornford EM, Hyman S, Cornford ME, Caron MJ (1996) Glut1 glucose transporter activity in human brain injury. *J Neurotrauma* 13:523-536.
32. Cortes R and Palacios JM (1986) Muscarinic cholinergic receptor subtypes in the rat brain. I. Quantitative autoradiographic studies. *Brain Res* 362:227-238.
33. Cortez SC, McIntosh TK, Noble LJ (1989) Experimental fluid percussion brain injury: vascular disruption and neuronal and glial alterations. *Brain Res* 482:271-282.
34. Costa DC Jones BE, Steiner TJ (1987) Relative ^{99m}Tc HMPAO and ^{11}3Sn microspheres distribution in dog brain. *Nuklearmedizin* 23 (suppl):498-500.
35. D'Argy R, Persson A and Sedvall G (1987) A quantitative cerebral and whole body autoradiographic study of a intravenously administered benzodiazepine antagonist [^{3}H]Ro 15-1788 in mice. *Psychopharmacology* 92:8-13.
36. D'Argy R, Gillberg PG, Stålnacke CG, Persson A, Bergström M, Långström B, Schoeps KO Aquilonius SM (1988) In vivo and in vitro receptor autoradiography of the human brain using an 11C-labeled benzodiazepine analogue. *Neurosci Lett* 85, 304-310.
37. Delahunty TM, Jiang JY, Gong QZ, Black RT, Lyeth BG (1995) Differential consequences of lateral and central fluid percussion brain injury on receptor coupling in rat hippocampus. *J Neurotrauma* 12:1045-1057.
38. Delforge J, Pappata S, Millet P, Samson Y, Bendriem B, Jobert A, Crouzel C, Syrota A (1995) Quantification of benzodiazepine receptors in human brain using PET, [^{11}C]flumazenil, and a single-experiment protocol. *J Cereb Blood Flow Metab* 15:284-300.
39. Dewar D, Graham DI (1996) Depletion of choline acetyltransferase activity but preservation of M1 and M2 muscarinic receptor binding sites in temporal cortex following head injury: a preliminary human postmortem study. *J Neurotrauma* 13:181-187.
40. DeWitt DS, Yuan XQ, Becker DP, Hayes RL (1988) Simultaneous, quantitative measurement of local blood flow and glucose utilization in tissue samples in normal and injured feline brain. *Brain Inj* 2:291-303.
41. DeWitt DS, Jenkins LW, Prough DS (1995) Enhanced vulnerability to secondary ischemic insults after experimental traumatic brain injury. *New Horiz* 3:376-383.
42. Di Chiro G, Brooks RA, Patronas NJ, Bairamian D, Kornblith PL, Smith BH, Mansi L, Barker J (1984) Issues in the in vivo measurement of glucose metabolism of human central nervous system tumors. *Ann Neurol* 15 S138-S146.
43. Dietrich WD, Alonso O, Busto R, Ginsberg MD (1994) Widespread metabolic depression and reduced somatosensory circuit activation following traumatic brain injury in rats. *J Neurotrauma* 11:629-640.
44. Dietrich WD, Alonso O, Busto R, Globus MY, Ginsberg MD (1994 *a*) Post-traumatic brain hypothermia reduces histopathological damage following concussive brain injury in the rat. *Acta Neuropathol (Berl)* 87:250-258.
45. Dietrich WD, Alonso O, Halley M (1994 *b*) Early microvascular and neuronal consequences of traumatic brain injury: a light and electron microscopic study in rats. *J Neurotrauma* 11:289-301.
46. Dietrich WD, Alonso O, Busto R, Prado R, Dewanjee S, Dewanjee MK, Ginsberg MD (1996) Widespread hemodynamic depression and focal platelet accumulation after fluid percussion brain injury: a double-label autoradiographic study in rats. *J Cereb Blood Flow Metab* 16:481-489.
47. Dietrich WD, Alonso O, Busto R, Prado R, Zhao W, Dewanjee MK, Ginsberg MD (1998) Posttraumatic cerebral ischemia after fluid percussion brain injury: an autoradiographic and histopathological study in rats. *Neurosurgery* 43:585-594.
48. Dixon CE, Lyeth BG, Povlishock JT, Findling RL, Hamm RJ, Marmarou A, Young HF, Hayes RL (1987) A fluid percussion model of experimental brain injury in the rat. *J Neurosurg* 67:110-119.
49. Dixon CE, Clifton GL, Lighthall JW, Yaghmai AA, Hayes RL (1991) A controlled cortical impact model of traumatic brain injury in the rat. *J Neurosci Methods* 39:253-262.
50. Dixon CE, Bao J, Johnson KM, Yang K, Whitson J, Clifton GL, Hayes RL (1995) Basal and scopolamine-evoked release of hippocampal acetylcholine following traumatic brain injury in rats. *Neurosci Lett*

198:111-114.
51. Dixon CE, Liu SJ, Jenkins LW, Bhattachargee M, Whitson JS, Yang K, Hayes RL (1995) Time course of increased vulnerability of cholinergic neurotransmission following traumatic brain injury in the rat. *Behav Brain Res* 70:125-131.
52. Duncan R, Patterson J, Macrae IM (1996) HMPAO as a regional cerebral blood flow tracer at high flow levels. *J Nucl Med* 37:661-664.
53. Dörje F, Wess J, Lambrecht G, Tacke R, Mutschler E, Brann MR (1991) Antagonist binding profiles of five cloned human muscarinic receptor subtypes. *J Pharmacol Exp Ther* 256:727-733.
54. Faden AI, Demediuk P, Panter SS, Vink R (1989) The role of excitatory amino acids and NMDA receptors in traumatic brain injury. *Science* 244(4906):798-800.
55. Farde L, Hall H, Pauli S and Halldin C (1995) Variability in D2-dopamine receptor density and affinity: a PET study with [^{11}C]raclopride in man. *Synapse* 20:200-208.
56. Farrell CL, Pardridge WM (1991) Blood-brain barrier glucose transporter is asymmetrically distributed on brain capillary endothelial lumenal and ablumenal membranes: an electron microscopic immunogold study. *Proc Natl Acad Sci U S A* 88:5779-5783.
57. Feeney DM, Boyeson MG, Linn RT, Murray HM, Dail WG (1981) Responses to cortical injury: I. Methodology and local effects of contusions in the rat. *Brain Res* 211:67-77.
58. Ferrarese C, Guidotti A, Costa E, Miletich RS, Rice KC, de Costa BR, Fulham MJ, DiChiro G (1991) In vivo study of NMDA-sensitive glutamate receptor by fluorothienylcycloexylpiperidine, a possible ligand for positron emission tomography. *Neuropharmacology* 30: 899-905.
59. Ferrari-DiLeo G, Waelbroeck M, Mash DC and Flynn DD (1994) Selective labeling and localization of the M4 (m4) muscarinic receptor subtype. *Mol Pharmacol 46*: 1028-1035.
60. Flynn DD, Reever CM, and Ferrari-DiLeo G (1997) Pharmacological strategies to selectively label and localize muscarinic receptor subtypes. *Drug Dev Res 40*: 104-116.
61. Foster AC, Wong EH (1987) The novel anticonvulsant MK-801 binds to the activated state of the N-methyl-D-aspartate receptor in rat brain. *Br J Pharmacol* 91:403-409.
62. Fox PT, Raichle ME, Mintun MA, Dence C (1988) Nonoxidative glucose consumption during focal physiologic neural activity. *Science* 241(4864):462-464.
63. Frackowiak RS, Lenzi GL, Jones T, Heather JD (1980) Quantitative measurement of regional cerebral blood flow and oxygen metabolism in man using ^{15}O and positron emission tomography: theory, procedure, and normal values. *J Comput Assist Tomogr* 4:727-736.
64. Frey KA, Ehrenkaufer RL, Agranoff BW (1985) Quantitative in vivo receptor binding. II. Autoradiographic imaging of muscarinic cholinergic receptors. *J Neurosci* 5:2407-2414.
65. Fukuda K, Tanno H, Okimura Y, Nakamura M, Yamaura A (1995) The blood-brain barrier disruption to circulating proteins in the early period after fluid percussion brain injury in rats. *J Neurotrauma* 12:315-324.
66. Fujibayashi Y, Cutler CS, Anderson CJ, McCarthy DW, Jones LA, Sharp T, Yonekura Y, Welch MJ (1999) Comparative studies of Cu-64-ATSM and C-11-acetate in an acute myocardial infarction model: ex vivo imaging of hypoxia in rats. *Nucl Med Biol* 26:117-121.
67. Gennarelli TA, Thibault LE, Adams JH, Graham DI, Thompson CJ, Marcincin RP (1982) Diffuse axonal injury and traumatic coma in the primate. *Ann Neurol* 12:564-574.
68. Gilbert RFT, Hanley MR and Iversen LL (1979) [^{3}H]-Quinuclidinyl benzilate binding to muscarinic receptors in rat brain: comparison of results from intact brain slices and homogenates. *Br J Pharmacol* 65:451-456.
69. Ginsberg MD, Howard BE, Hassel WR (1984) Emission tomographic measurement of local cerebral blood flow in humans by an in vivo autoradiographic strategy. *Ann Neurol* 15 Suppl:S12-18.
70. Ginsberg MD, Zhao W, Alonso OF, Loor-Estades JY, Dietrich WD, Busto R (1997) Uncoupling of local cerebral glucose metabolism and blood flow after acute fluid-percussion injury in rats. *Am J Physiol* 272:H2859-H2868.
71. Gjedde A (1987) Does deoxyglucose uptake in the brain reflect energy metabolism? *Biochem Pharmacol* 36:1853-1861.
72. Globus MY, Alonso O, Dietrich WD, Busto R, Ginsberg MD (1995) Glutamate release and free radical production following brain injury: effects of posttraumatic hypothermia. *J Neurochem* 65:1704-1711.
73. Goeders NE and Kuhar MJ (1985) Benzodiazepine receptor binding in vivo with [^{3}H]Ro 15-1788. *Life Sci* 37:345-355.
74. Gorman LK, Fu K, Hovda DA, Becker DP, Katayama Y (1989) Analysis of acetylcholine release following concussive brain injury in the rat. *J Neurotrauma* 6:203.
75. Gorman LK, Fu K, Hovda DA, Murray M, Traystman RJ (1996) Effects of traumatic brain injury on the cholinergic system in the rat. *J Neurotrauma* 13:457-463.
76. Gray SM, Adams V, Yamashita Y, Le SP, Goddard-Finegold J, McCabe ER (1994) Hexokinase binding in ischemic and reperfused piglet brain. *Biochem Med Metab Biol* 53:145-148.
77. Greenberg JH, Hamar J, Welsh FA, Harris V, Reivich M (1992) Effect of ischemia and reperfusion on λ of the lumped constant of the [^{14}C]deoxyglucose technique. *J Cereb Blood Flow Metab* 12:70-77.

78. Griffiths T, Evans MC, Meldrum BS (1983) Intracellular calcium accumulation in rat hippocampus during seizures induced by bicuculline or L-allylglycine. *Neuroscience* 10:385-395.
79. Griffiths T, Evans MC, Meldrum BS (1984) Status epilepticus: the reversibility of calcium loading and acute neuronal pathological changes in the rat hippocampus. *Neuroscience* 12:557-567.
80. Göller L, Bergström M, Nilsson S, Westerberg G and Långström B (1995) MAO-A enzyme binding in bladder cancer characterized with [^{11}C]harmine in frozen section autoradiography. *Oncol Rep* 2:717-721.
81. Hall H, Wedel I, Halldin C, Kopp J and Farde L (1990) Comparison of the in vitro receptor binding properties of N-[^{3}H]methylspiperone and [^{3}H]raclopride to rat and human brain membranes. *J Neurochem* 55:2048-2057.
82. Hall H, Litton JE, Halldin C, Kopp J and Sedvall G (1992) Studies on the binding of [^{3}H]flumazenil and [^{3}H]sarmazenil in post-mortem human brain. *Human Psychopharmacology* 7:367-377.
83. Hall H, Halldin C, Farde L, Sedvall G (1998) Whole hemisphere autoradiography of the postmortem human brain. *Nucl Med Biol* 25:715-719.
84. Hamm RJ, O'Dell DM, Pike BR, Lyeth BG (1993) Cognitive impairment following traumatic brain injury: the effect of pre- and post-injury administration of scopolamine and MK-801. *Brain Res Cogn Brain Res* 1:223-226.
85. Hansen TD, Warner DS, Todd MM, Baker MT and Jensen NF (1991) The influence of inhalational anesthetics on in vivo and in vitro benzodiazepine receptor binding in the rat cerebral cortex. *Anesthesiology* 74:97-104.
86. Hantraye P, Kalhma M, Prenant C, Guibert B, Sastre J, Crouzei M, Naquet R, Comar D and Maziere M (1984) Central type benzodiazepine binding sites: a positron emission tomography study in the baboon's brain. *Neurosci Lett* 48:115-120.
87. Harrell LE, Barlow TS, Parsons D (1987) Cholinergic neurons, learning, and recovery of function. *Behav Neurosci* 101:644-652, 743.
88. Hartvig P, Valtysson J, Antoni G, Westerberg G, Långström B, Ratti Moberg E, Øye I (1994) Brain kinetics of (R)- and (S)-[N-methyl-^{11}C]ketamine in the rhesus monkey studied by positron emission tomography (PET). *Nucl Med Biol* 21:927-934.
89. Hartvig P, Valtysson J, Lindner KJ, Kristensen J, Karlsten R, Gustafsson LL, Persson J, Svensson JO, Ø ye I, Antoni G, Westerberg G, Långström B (1995) Central nervous system effects of subdissociative doses of (S)-ketamine are related to plasma and brain concentrations measured with positron emission tomography in healthy volunteers. *Clin Pharmacol Ther* 58:165-173.
90. Hawkins RA, Miller AL, Cremer JE, Veech RL (1974) Measurement of the rate of glucose utilization by rat brain in vivo. *J Neurochem* 23:917-923.
91. Hawkins RA, Mans AM, Davis DW, Vina JR, Hibbard LS (1985) Cerebral glucose use measured with [^{14}C]glucose labeled in the 1, 2, or 6 position. *Am J Physiol* 248:C170-176.
92. Hawkins RA, Mans AM, Davis DW, DeJoseph MR (1988) Comparison of [^{14}C]glucose and [^{14}C]deoxyglucose as tracers of brain glucose use. *Am J Physiol* 254:E310-317.
93. Hawkins RA, Hawkins PA, Mans AM, Vina JR, DeJoseph MR (1994) Optimizing the measurement of regional cerebral glucose consumption with [6-^{14}C]glucose. *J Neurosci Methods* 54:49-62.
94. Hayes RL, Jenkins LW, Lyeth BG, Balster RL, Robinson SE, Clifton GL, Stubbins JF, Young HF (1988) Pretreatment with phencyclidine, an N-methyl-D-aspartate antagonist, attenuates long-term behavioral deficits in the rat produced by traumatic brain injury. *J Neurotrauma* 5:259-274.
95. Hayes RL, Katayama Y, Jenkins LW, Lyeth BG, Clifton GL, Gunter J, Povlishock JT, Young HF (1988) Regional rates of glucose utilization in the cat following concussive head injury. *J Neurotrauma* 5:121-137.
96. Heath DL, Vink R (1998) Neuroprotective effects of MgSO4 and MgCl2 in closed head injury: a comparative phosphorus NMR study. *J Neurotrauma* 15:183-189.
97. Heiss WD, Graf R, Fujita T, Ohta K, Bauer B, Lottgen J, Wienhard K (1997) Early detection of irreversibly damaged ischemic tissue by flumazenil positron emission tomography in cats. *Stroke* 28:2045-2052.
98. Heiss WD, Grond M, Thiel A, Ghaemi M, Sobesky J, Rudolf J, Bauer B, Wienhard K (1998) Permanent cortical damage detected by flumazenil positron emission tomography in acute stroke. *Stroke* 29:454-461.
99. Heiss WD, Kracht L, Grond M, Rudolf J, Bauer B, Wienhard K, Pawlik G (2000) Early [^{11}C]Flumazenil/H_2O positron emission tomography predicts irreversible ischemic cortical damage in stroke patients receiving acute thrombolytic therapy. *Stroke* 31:366-369.
100. Hepler DJ, Olton DS, Wenk GL, Coyle JT (1985) Lesions in nucleus basalis magnocellularis and medial septal area of rats produce qualitatively similar memory impairments. *J Neurosci* 5:866-873.
101. Hepler DJ, Wenk GL, Cribbs BL, Olton DS, Coyle JT (1985) Memory impairments following basal forebrain lesions. *Brain Res* 346:8-14.
102. Hicks R, Soares H, Smith D, McIntosh T (1996) Temporal and spatial characterization of neuronal injury following lateral fluid-percussion brain injury in the rat. *Acta Neuropathol (Berl)* 91:236-246.
103. Hillered L, Hallström A, Segersvärd S, Persson L, Ungerstedt U (1989) Dynamics of extracellular metabolites in the striatum after middle cerebral artery occlusion in the rat monitored by intracerebral microdialysis. *J Cereb Blood Flow Metab* 9:607-616.

104. Hillered L, Persson L, Ponten U, Ungerstedt U (1990) Neurometabolic monitoring of the ischaemic human brain using microdialysis. *Acta Neurochir (Wien)* 102:91-97.
105. Hillered L and Persson L (1999) Neurochemical monitoring of the acutely injured human brain. *Scand J Clin Lab Invest* 59(Suppl229):9-18.
106. Hostetler KY, Landau BR (1967) Estimation of the pentose cycle contribution to glucose metabolism in tissue in vivo. *Biochemistry* 6:2961-2964.
107. Hovda DA, Yoshino A, Kawamata T, Katayama Y, Fineman I, Becker DP (1990) The increase in local cerebral glucose utilization following fluid percussion brain injury is prevented with kynurenic acid and is associated with an increase in calcium. *Acta Neurochir Suppl (Wien)* 51:331-333.
108. Hovda DA, Yoshino A, Kawamata T, Katayama Y, Becker DP (1991) Diffuse prolonged depression of cerebral oxidative metabolism following concussive brain injury in the rat: a cytochrome oxidase histochemistry study. *Brain Res* 567:1-10.
109. Hovda DA, Lee SM, Smith ML, Von Stuck S, Bergsneider M, Kelly D, Shalmon E, Martin N, Caron M, Mazziotta J, Phelps M, Becker DP (1995) The neurochemical and metabolic cascade following brain injury: moving from animal models to man. *J Neurotrauma* 12:903-906.
110. Howard BE, Ginsberg MD, Hassel WR, Lockwood AH, Freed P (1983) On the uniqueness of cerebral blood flow measured by the in vivo autoradiographic strategy and positron emission tomography. *J Cereb Blood Flow Metab* 3:432-441.
111. Hucker HB, Hutt JE, White SD, Arison BH, Zacchei AG (1983) Disposition and metabolism of (+)-5-methyl-10,11-dihydro-5H-dibenzo[a,d] cyclohepten-5,10-imine in rats, dogs and monkeys. *Drug Metab Dispos* 11: 54-58.
112. Huettner JE, Bean BP (1988) Block of N-methyl-D-aspartate-activated current by the anticonvulsant MK-801: selective binding to open channels. *Proc Natl Acad Sci U S A* 85:1307-1311
113. Hulme EC, Birdsall NJ, Buckley NJ (1990) Muscarinic receptor subtypes. *Annu Rev Pharmacol Toxicol* 30:633-673.
114. Hulme EC and Birdsall NJM. (1993) Strategy and tactics in receptor binding studies. *In Receptor-Ligand-Interactions, A Practical Approach (Edited by Hulme E. C.),* pp. 63-176. Oxford University Press, Oxford, UK.
115. Humayun MS, Presty SK, Lafrance ND, Holcomb HH, Loats H, Long DM, Wagner HN, Gordon B (1989) Local cerebral glucose abnormalities in mild closed head injured patients with cognitive impairments. *Nucl Med Commun* 10:335-344.
116. Höglund AU and Baghdoyan HA (1997) M2, M3 and M4 but not M1, muscarinic receptor subtypes are present in rat spinal cord. *J Pharmacol Exp Ther* 281:470-477.
117. Inao S, Marmarou A, Clarke GD, Andersen BJ, Fatouros PP, Young HF (1988) Production and clearance of lactate from brain tissue, cerebrospinal fluid, and serum following experimental brain injury. *J Neurosurg* 69:736-744.
118. Ishiwata K, Hayakawa N, Ogi N, Oda K, Toyama H, Endo K, Tanaka A, Senda M (1999) Comparison of three PET dopamine D_2-like receptor ligands, [^{11}C]raclopride, [^{11}C]nemonapride and [^{11}C]N-methylspiperone, in rats. *Ann Nucl Med* 13:161-167.
119. Ishiwata K, Ogi N, Tanaka A, Senda M (1999) Quantitative ex vivo and in vitro receptor autoradiography using ^{11}C-labeled ligands and an imaging plate: a study with a dopamine D2-like receptor ligand [^{11}C]nemonapride. *Nucl Med Biol* 26:291-296.
120. Ishiwata K, Noguchi J, Wakabayashi S, Shimada J, Ogi N, Nariai T, Tanaka A, Endo K, Suzuki F, Senda M (2000) ^{11}C-Labeled KF18446: a potential central nervous system adenosine A_{2a} receptor ligand. *J Nucl Med* 41:345-354.
121. Jenkins LW, Moszynski K, Lyeth BG, Lewelt W, DeWitt DS, Allen A, Dixon CE, Povlishock JT, Majewski TJ, Clifton GL, et al (1989) Increased vulnerability of the mildly traumatized rat brain to cerebral ischemia: the use of controlled secondary ischemia as a research tool to identify common or different mechanisms contributing to mechanical and ischemic brain injury. *Brain Res* 477:211-224.
122. Jones SC, Greenberg JH, Reivich M (1982) Error analysis for the determination of cerebral blood flow with the continuous inhalation of ^{15}O-labeled carbon dioxide and positron emission tomography. *J Comput Assist Tomogr* 6:116-124.
123. Jiang JY, Lyeth BG, Delahunty TM, Phillips LL, Hamm RJ (1994) Muscarinic cholinergic receptor binding in rat brain at 15 days following traumatic brain injury. *Brain Res* 651:123-128.
124. Jiang XB, Ohno K, Qian L, Tominaga B, Kuroiwa T, Nariai T, Hirakawa K (2000) Changes in local cerebral blood flow, glucose utilization, and mitochondrial function following traumatic brain injury in rats. *Neurol Med Chir (Tokyo)* 40:16-29.
125. Johnston RF, Pickett SC, Barker DL (1990) Autoradiography using storage phosphor technology. *Electrophoresis* 11, 355-360.
126. Jolkkonen M, van Giersbergen PLM, Hellman U, Wernstedt C and Karlsson E (1994) A toxin from the green mamba *dendroaspis angusticepts:* amino acid sequence and selectivity for muscarinic m4 receptors. *FEBS Lett* 352:91-94.
127. Kapoor R, Spence AM, Muzi M, Graham MM, Abbott GL, Krohn KA (1989) Determination of the

deoxyglucose and glucose phosphorylation ratio and the lumped constant in rat brain and a transplantable rat glioma. *J Neurochem* 53:37-44.
128. Katayama Y, Becker DP, Tamura T, Hovda DA (1990) Massive increases in extracellular potassium and the indiscriminate release of glutamate following concussive brain injury. *J Neurosurg* 73:889-900.
129. Katayama Y, Maeda T, Koshinaga M, Kawamata T, Tsubokawa T (1995) Role of excitatory amino acid-mediated ionic fluxes in traumatic brain injury. *Brain Pathol* 5:427-435.
130. Kawamata T, Katayama Y, Hovda DA, Yoshino A, Becker DP (1992) Administration of excitatory amino acid antagonists via microdialysis attenuates the increase in glucose utilization seen following concussive brain injury. *J Cereb Blood Flow Metab* 12:12-24.
131. Kawamata T, Katayama Y, Hovda DA, Yoshino A, Becker DP (1995) Lactate accumulation following concussive brain injury: the role of ionic fluxes induced by excitatory amino acids. *Brain Res* 674:196-204.
132. Kemp JA, Foster AC, Wong EHF (1987) Non-competitive antagonists of excitatory amino acid receptors *Trends Neurosci* 10:294-298.
133. Kleckner NW, Dingledine R (1988) Requirement for glycine in activation of NMDA-receptors expressed in Xenopus oocytes. *Science* 241(4867):835-837.
134. Kloog Y, Egozi Y, Sokolovsky M (1979) Characterization of muscarinic acetylcholine receptors from mouse brain: evidence for regional heterogeneity and isomerization. *Mol Pharmacol* 15:545-558.
135. Kloog Y, Sokolovsky M (1977) Muscarinic acetylcholine receptors interactions: competition binding studies with agonists and antagonists. *Brain Res* 134:167-172.
136. Komiskey HL and MacFarlan MF (1983) Aging: effect on neuronal and non-neuronal benzodiazepine binding sites. *Neurochem. Res*. 8, 1135-1141.
137. Krieglstein J, Sperling G, Twietmeyer G (1981) Effects of thiopental on regulatory mechanisms of brain energy metabolism. Naunyn Schmiedebergs Arch Pharmacol 318:56-61.
138. Kroppenstedt SN, Schneider GH, Thomale UW, Unterberg AW (1998) Protective effects of aptiganel HCl (Cerestat®) following controlled cortical impact injury in the rat. *J Neurotrauma* 15:191-197.
139. Kuhar MJ (1985) Receptor localization with the microscope, in: *Neurotransmitter Receptor Binding* (Yamamura HI, Enna SJ and Kuhar MJ eds) pp 153-176, Raven Press.
140. Kumlien E, Hartvig P, Valind S, Øye I, Tedroff J, Långström B (1999) NMDA-receptor activity visualized with (S)-[N-methyl-^{11}C]ketamine and positron emission tomography in patients with medial temporal lobe epilepsy. *Epilepsia* 40:30-37.
141. Langfitt TW, Obrist WD, Alavi A, Grossman RI, Zimmerman R, Jaggi J, Uzzell B, Reivich M, Patton DR (1986) Computerized tomography, magnetic resonance imaging, and positron emission tomography in the study of brain trauma. Preliminary observations. *J Neurosurg* 64:760-767.
142. Lear JL, Ackermann RF (1988) Comparison of cerebral glucose metabolic rates measured with fluorodeoxyglucose and glucose labeled in the 1, 2, 3-4, and 6 positions using double label quantitative digital autoradiography. *J Cereb Blood Flow Metab* 8:575-785.
143. Lear JL, Ackermann RF (1989) Regional comparison of the lumped constants of deoxyglucose and fluorodeoxyglucose. *Metab Brain Dis* 4:95-104.
144. Lear JL (1988) Initial cerebral HM-PAO distribution compared to LCBF: use of a model which considers cerebral HM-PAO trapping kinetics. *J Cereb Blood Flow Metab* 8:S31-37
145. Levasseur JE, Alessandri B, Reinert M, Bullock R, Kontos HA (2000) Fluid percussion injury transiently increases then decreases brain oxygen consumption in the rat. *J Neurotrauma* 17:101-112.
146. Lewelt W, Jenkins LW, Miller JD (1980) Autoregulation of cerebral blood flow after experimental fluid percussion injury of the brain. *J Neurosurg* 53:500-511.
147. Loo P, Braunwalder A, Lehmann J, Williams M (1986) Radioligand binding to central phencyclidine recognition sites is dependent on excitatory amino acid receptor agonists. *Eur J Pharmacol* 123:467-468.
148. Lu DM, Davis DW, Mans AM, Hawkins RA (1983) Regional cerebral glucose utilization measured with [14C]glucose in brief experiments. *Am J Physiol* 245:C428-C438.
149. Lyeth BG, Ray M, Hamm RJ, Schnabel J, Saady JJ, Poklis A, Jenkins LW, Gudeman SK, Hayes RL (1992) Postinjury scopolamine administration in experimental traumatic brain injury. *Brain Res* 569:281-286.
150. Lyeth BG, Jiang JY, Delahunty TM, Phillips LL, Hamm RJ (1994) Muscarinic cholinergic receptor binding in rat brain following traumatic brain injury. *Brain Res* 640:240-245.
151. Långström B (1990) Design of molecules labeled with β^+ emitters for use in multitracer investigations using positron emission tomography. *Acta Radiol Suppl* 374:47-51.
152. Martin DC, Abraham JE, Plagenhoef M, Aronstam RS (1991) Volatile anesthetics and NMDA receptors. Enflurane inhibition of glutamate-stimulated [^{3}H]MK-801 binding and reversal by glycine. *Neurosci Lett* 132: 73-76.
153. Martin DC, Plagenhoef M, Abraham J, Dennison RL, Aronstam RS (1995) Volatile anesthetics and glutamate activation of N-methyl-D-aspartate receptors. *Biochem Pharmacol* 49: 809-817.
154. Matsuda H, Tsuji S, Oba H, Imai K, Shiba K, Terada H, Seki H, Sumiya H, Mori H, Hisada K (1988) Direct autoradiographic comparison of ^{99m}Tc-HMPAO with ^{125}I-IMP in experimental brain ischaemia. *Nucl Med Commun* 9:891-897.

155. Matsumoto A, Namon R, Utsunomiya Y, Kogure K, Scheinberg P, Reinmuth OM (1975) The measurement of cerebral blood flow in the rat. *Stroke* 6:630-637.
156. Maxwell WL, Hardy IG, Watt C, McGadey J, Graham DI, Adams JH, Gennarelli TA (1992) Changes in the choroid plexus, responses by intrinsic epiplexus cells and recruitment from monocytes after experimental head acceleration injury in the non-human primate. *Acta Neuropathol (Berl)* 84:78-84.
157. Maxwell WL, Whitfield PC, Suzen B, Graham DI, Adams JH, Watt C, Gennarelli TA (1992) The cerebrovascular response to experimental lateral head acceleration. *Acta Neuropathol (Berl)* 84:289-296.
158. Mayer ML, Westbrook GL, Guthrie PB (1984) Voltage-dependent block by Mg2+ of NMDA responses in spinal cord neurones. *Nature* 309(5965):261-263.
159. Maziere M, Hantraye P, Prenant C, Sastre J, Comar D (1984) Synthesis of ethyl 8-fluoro-5,6-dihydro-5-[^{11}C]methyl-6-oxo-4H-imidazo [1,5-a] [1,4]benzodiazepine-3-carboxylate (RO 15.1788-^{11}C): a specific radioligand for the in vivo study of central benzodiazepine receptors by positron emission tomography. *Int J Appl Radiat Isot* 35:973-976.
160. McCulloch J, Wallace MC, Laurie D, Angerson WJ, Burns HD, Gibson RE (1992) Imaging activation in the NMDA receptor complex with ^{125}Iodo-MK-801, in *Pharmacology of cerebral ischaemia* (Kreiglstein J, Oberpichler-Schwenk H, eds), pp 59-64. Wissenschaftliche Verlagsgesellschaft mbH, Stuttgart.
161. McIntosh TK, Faden AI, Bendall MR, Vink R (1987) Traumatic brain injury in the rat: alterations in brain lactate and pH as characterized by ^{1}H and ^{31}P nuclear magnetic resonance. *J Neurochem* 49:1530-1540.
162. McIntosh TK, Faden AI, Yamakami I, Vink R (1988) Magnesium deficiency exacerbates and pretreatment improves outcome following traumatic brain injury in rats: 31P magnetic resonance spectroscopy and behavioral studies. *J Neurotrauma* 5:17-31.
163. McIntosh TK, Vink R, Noble L, Yamakami I, Fernyak S, Soares H, Faden AL (1989 *a*) Traumatic brain injury in the rat: characterization of a lateral fluid-percussion model. *Neuroscience* 28:233-244.
164. McIntosh TK, Vink R, Yamakami I, Faden AI (1989 *b*) Magnesium protects against neurological deficit after brain injury. *Brain Res* 482:252-260.
165. McIntosh TK, Vink R, Soares H, Hayes R, Simon R (1990) Effect of noncompetitive blockade of N-methyl-D-aspartate receptors on the neurochemical sequelae of experimental brain injury. *J Neurochem* 55:1170-1179.
166. McIntosh TK (1994) Neurochemical sequelae of traumatic brain injury: therapeutic implications. *Cerebrovasc Brain Metab Rev* 6:109-162.
167. McIntosh TK, Juhler M, Wieloch T (1998) Novel pharmacologic strategies in the treatment of experimental traumatic brain injury: 1998. *J Neurotrauma* 15:731-769.
168. McPherson GA (1994) Radlig, A collection of programs for the analysis of radioligand binding experiments. *Biosoft, Cambridge, UK*.
169. Meldrum B, Garthwaite J (1990) Excitatory amino acid neurotoxicity and neurodegenerative disease. *Trends Pharmacol Sci* 11:379-387.
170. Meldrum BS, Swan JH, Leach MJ, Millan MH, Gwinn R, Kadota K, Graham SH, Chen J, Simon RP (1992) Reduction of glutamate release and protection against ischemic brain damage by BW 1003C87. *Brain Res* 593:1-6.
171. Metherate R, Ashe JH, Weinberger NM (1990) Acetylcholine modifies neuronal acoustic rate-level functions in guinea pig auditory cortex by an action at muscarinic receptors. *Synapse* 6:364-368.
172. Miller LG, Deutsch SI, Greenblatt DJ, Paul SM, Shader RI (1988) Acute barbiturate administration increases benzodiazepine receptor binding in vivo. *Psychopharmacology (Berl)* 96:385-390.
173. Miller LP, Lyeth BG, Jenkins LW, Oleniak L, Panchision D, Hamm RJ, Phillips LL, Dixon CE, Clifton GL, Hayes RL (1990) Excitatory amino acid receptor subtype binding following traumatic brain injury. *Brain Res* 526:103-107.
174. Miyamoto M, Kato J, Narumi S, Nagaoka A (1987) Characteristics of memory impairment following lesioning of the basal forebrain and medial septal nucleus in rats. *Brain Res* 419:19-31.
175. Monaghan DT, Cotman CW (1985) Distribution of *N*-Methyl-D-aspartate-sensitive L-[^{3}H]glutamate-binding sites in rat brain. *J Neurosci* 5: 2909-2919.
176. Mulholland GK, Jewett, DW, Otto CA, Kilbourn MR, Sherman PS and Kuhl DE (1988) Synthesis and regional brain distribution of [C-11]*N*-methyl-4-piperidyl benzilate ([C-11]NMPB) in the rat. *J Nucl Med* 29:768.
177. Mulholland GK, Kilbourn MR, Sherman P, Carey JE, Frey KA, Koeppe RA, Kuhl DE (1995) Synthesis, in vivo biodistribution and dosimetry of [^{11}C]N-methylpiperidyl benzilate ([^{11}C]NMPB), a muscarinic acetylcholine receptor antagonist. *Nucl Med Biol* 22:13-17.
178. Murata T, Matsumura K, Onoe H, Bergström M, Takechi H, Sihver S, Sihver W, Neu H, Andersson Y, Ögren M, Fast K-J, Långström B and Watanabe Y (1996) Receptor imaging technique with ^{11}C-labeled receptor ligands in living brain slices: its application to time-resolved imaging and saturation analysis of benzodiazepine receptor using [^{11}C]Ro15-1788. *Neurosci Res* 25:145-154.
179. Murata T, Matsumura K, Sihver S, Onoe H, Bergström M, Sihver W, Yonekura Y, Långström B and Watanabe Y. (1998) Triazolam-induced modulation of muscarinic acetylcholine receptor in living brain slices as revealed by a new positron-based imaging technique. *J Neural Transm* 105:1117-1127.

180. Murata T, Omata N, Fujibayashi Y, Waki A, Sadato N, Yoshimoto M, Omori M, Isaki K, Yonekura Y (1999) Dynamic changes in glucose metabolism induced by thiamine deficiency and its replenishment as revealed by a positron autoradiography technique using rat living brain slices. *J Neurol Sci* 164:29-36.
181. Murata T, Omata N, Fujibayashi Y, Waki A, Sadato N, Yoshida S, Yano R, Yoshimoto M, Yonekura Y (1999) Dynamic changes in glucose metabolism of living rat brain slices induced by hypoxia and neurotoxic chemical-loading revealed by positron autoradiography. *J Neural Transm* 106:1075-1087.
182. Murata T, Waki A, Omata N, Fujibayashi Y, Sadato N, Yano R, Yoshimoto M, Isaki K, Yonekura Y (1998) Dynamic changes in glucose metabolism by lactate loading as revealed by a positron autoradiography technique using rat living brain slices. *Neurosci Lett* 249:155-158.
183. Möhler H and Okada T (1977) Benzodiazepine receptor: demonstration in the central nervous system. *Science* 198, 849-851.
184. Möhler H, Burkard WP, Keller HH, Richards JG and Haefely W (1981) Benzodiazepine antagonist Ro15-1788: binding characteristics and interaction with drug-induced changes in dopamine turnover and cerebellar cGMP levels. *J Neurochem* 37:714-722.
185. Möhler H and Richards JG (1981) Agonist and antagonist benzodiazepine receptor interaction in vitro. *Nature* 294:763-765.
186. Möhler H (1982) Benzodiazepine receptors: differential interaction of benzodiazepine agonists and antagonists after photoaffinity labeling with flunitrazepam. *Eu J Pharmacol* 80:435-436.
187. Nakai H, Matsuda H, Takara E, Diksic M, Yamamoto YL, Meyer E, Redies C (1988) Changes in lumped and rate constants in experimental cerebral ischemia--intra-animal comparison before and after middle cerebral artery occlusion. *Neurol Med Chir (Tokyo)* 28:11-17.
188. Neirinckx RD, Canning LR, Piper IM, Nowotnik DP, Pickett RD, Holmes RA, Volkert WA, Forster AM, Weisner PS, Marriott JA (1987) Technetium-99m d,l-HM-PAO: a new radiopharmaceutical for SPECT imaging of regional cerebral blood perfusion. *J Nucl Med* 28:191-202.
189. Nilsson B, Nordström CH (1977) Experimental head injury in the rat. Part 3: Cerebral blood flow and oxygen consumption after concussive impact acceleration. *J Neurosurg* 47:262-273.
190. Nilsson B, Ponten U, Voigt G (1977) Experimental head injury in the rat. Part 1: Mechanics, pathophysiology, and morphology in an impact acceleration trauma model. *J Neurosurg* 47:241-251.
191. Nilsson P, Hillered L, Ponten U, Ungerstedt U (1990) Changes in cortical extracellular levels of energy-related metabolites and amino acids following concussive brain injury in rats. *J Cereb Blood Flow Metab* 10:631-637.
192. Nilsson P, Hillered L, Olsson Y, Sheardown MJ, Hansen AJ (1993) Regional changes in interstitial K^+ and Ca^{2+} levels following cortical compression contusion trauma in rats. *J Cereb Blood Flow Metab* 13:183-192.
193. O'Dell DM, Gibson CJ, Wilson MS, DeFord SM, Hamm RJ (2000) Positive and negative modulation of the GABA(A) receptor and outcome after traumatic brain injury in rats. *Brain Res* 861:325-332.
194. Olney JW, Ho OL, Rhee V (1971) Cytotoxic effects of acidic and sulphur containing amino acids on the infant mouse central nervous system. *Exp Brain Res* 14:61-76.
195. Olney J, Price M, Salles KS, Labruyere J, Frierdich G (1987) MK-801 powerfully protects against N-methyl aspartate neurotoxicity. *Eur J Pharmacol* 141:357-261.
196. Omata N, Murata T, Fujibayashi Y, Waki A, Sadato N, Yoshimoto M, Wada Y, Yonekura Y (2000) Hypoxic but not ischemic neurotoxicity of free radicals revealed by dynamic changes in glucose metabolism of fresh rat brain slices on positron autoradiography. *J Cereb Blood Flow Metab* 20:350-358.
197. Orzi F, Lucignani G, Dow-Edwards D, Namba H, Nehlig A, Patlak CS, Pettigrew K, Schuier F, Sokoloff L (1988) Local cerebral glucose utilization in controlled graded levels of hyperglycemia in the conscious rat. *J Cereb Blood Flow Metab* 8:346-356.
198. Owens J, Wyper DJ, Patterson J, Brown DR, Elliott AT, Teasdale GM, McCulloch J (1997) First SPET images of glutamate (NMDA) receptor activation in vivo in cerebral ischaemia. *Nucl Med Commun* 18:149-158.
199. Parry DM, Pedersen PL (1990) Glucose catabolism in brain. Intracellular localization of hexokinase. *J Biol Chem 265:1059-1066*.
200. Paxinos G, Watson C (1982) The Rat Brain in Stereotaxic Coordinates. *Academic Press, Inc., New York*.
201. Persson A, Ehrin E, Eriksson L, Farde L, Hedström CG, Litton JE, Mindus P and Sedvall G (1985) Imaging of ^{11}C-labelled Ro 15-1788 binding to benzodiazepine receptors in the human brain by positron emission tomography. *J Psychiatr Res* 19:609-622.
202. Persson L, Valtysson J, Enblad P, Warme PE, Cesarini K, Lewen A, Hillered L (1996) Neurochemical monitoring using intracerebral microdialysis in patients with subarachnoid hemorrhage. *J Neurosurg* 84:606-616.
203. Phelps ME, Huang SC, Hoffman EJ, Selin C, Sokoloff L, Kuhl DE (1979) Tomographic measurement of local cerebral glucose metabolic rate in humans with (F-18)2-fluoro-2-deoxy-D-glucose: validation of method. *Ann Neurol* 6:371-388.
204. Phillips LL, Lyeth BG, Hamm RJ, Jiang JY, Povlishock JT, Reeves TM (1997) Effect of prior receptor antagonism on behavioral morbidity produced by combined fluid percussion injury and entorhinal cortical

lesion. *J Neurosci Res* 49:197-206.
205. Pike BR, Hamm RJ (1995) Post-injury administration of BIBN 99, a selective muscarinic M2 receptor antagonist, improves cognitive performance following traumatic brain injury in rats. *Brain Res* 686:37-43.
206. Pike BR, Hamm RJ (1997) Chronic administration of a partial muscarinic M1 receptor agonist attenuates decreases in forebrain choline acetyltransferase immunoreactivity following experimental brain trauma. *Exp Neurol* 147:55-65.
207. Price GW, Ahier RG, Middlemiss DN, Singh L, Tricklebank MD, Wong EH (1988) In vivo labelling of the NMDA receptor channel complex by [^{3}H]MK-801. *Eur J Pharmacol* 158:279-282.
208. Raghupathi R, Welsh FA, Lowenstein DH, Gennarelli TA, McIntosh TK (1995) Regional induction of c-fos and heat shock protein-72 mRNA following fluid-percussion brain injury in the rat. *J Cereb Blood Flow Metab* 15:467-473.
209. Ransom RW, Stec NL (1988) Cooperative modulation of [^{3}H]MK-801 binding to the N-methyl-D-aspartate receptor-ion channel complex by L-glutamate, glycine, and polyamines. *J Neurochem* 51:830-836.
210. Reivich M, Kuhl D, Wolf A, Greenberg J, Phelps M, Ido T, Casella V, Fowler J, Hoffman E, Alavi A, Som P, Sokoloff L (1979) The [^{18}F]fluorodeoxyglucose method for the measurement of local cerebral glucose utilization in man. *Circ Res* 44:127-137.
211. Richards JG, Möhler H, and Haefely W (1982) Benzodiazepine binding sites: receptors or acceptors? *Trend. Pharmac.* Sci. 3, 233-235.
212. Richards JG and Möhler H (1984) Benzodiazepine receptors. *Neuropharmacology* 23:233-242.
213. Riche D, Hantraye P, Guibert B, Naquet R, Loc'h C, Maziere B, and Maziere M (1998) Anatomical atlas of the baboon's brain in the orbito-meatal plane used in experimental positron emission tomography. *Brain Res Bull* 20:283-301.
214. Rudolf J, Sobesky J, Grond M, Heiss WD (2000) Identification by positron emission tomography of neuronal loss in acute vegetative state. *Lancet* 355:115-116.
215. Saija A, Hayes RL, Lyeth BG, Dixon CE, Yamamoto T, Robinson SE (1988) The effect of concussive head injury on central cholinergic neurons. *Brain Res* 452:303-311.
216. Saija A, Robinson SE, Lyeth BG, Dixon CE, Yamamoto T, Clifton GL, Hayes RL (1988) The effects of scopolamine and traumatic brain injury on central cholinergic neurons. *J Neurotrauma* 5:161-170.
217. Sakurai SY, Cha JH, Penney JB, Young AB (1991) Regional distribution and properties of [^{3}H]MK-801 binding sites determined by quantitative autoradiography in rat brain. *Neuroscience* 40:533-43
218. Sanger DJ and Benavides J (1993) Discriminative stimulus effects of ω (BZ) receptor ligands: correlation with in vivo inhibition of [^{3}H]flumazenil binding in different regions of the rat central nervous system. *Psychopharmacology* 111:315-322.
219. Saunders ML, Miller JD, Stablein D, Allen G (1979) The effects of graded experimental trauma on cerebral blood flow and responsiveness to CO_2. *J Neurosurg* 51:18-26.
220. Schmidt RH, Grady MS (1995) Loss of forebrain cholinergic neurons following fluid-percussion injury: implications for cognitive impairment in closed head injury. *J Neurosurg* 83:496-502.
221. Schwartz RD, Huff RA, Yu X, Carter ML, Bishop M (1994) Postischemic diazepam is neuroprotective in the gerbil hippocampus. *Brain Res* 647:153-160.
222. Scremin OU, Li MG, Jenden DJ (1997) Cholinergic modulation of cerebral cortical blood flow changes induced by trauma. *J Neurotrauma* 14:573-586.
223. Sette G, Baron JC, Young AR, Miyazawa H, Tillet I, Barre L, Travere JM, Derlon JM, MacKenzie ET (1993) In vivo mapping of brain benzodiazepine receptor changes by positron emission tomography after focal ischemia in the anesthetized baboon. *Stroke* 24:2046-2058
224. Shah KR, West M (1983) The effect of concussion on cerebral uptake of 2-deoxy-D-glucose in rat. *Neurosci Lett* 40:287-291.
225. Sharples PM, Stuart AG, Matthews DS, Aynsley-Green A, Eyre JA (1995) Cerebral blood flow and metabolism in children with severe head injury. Part 1: Relation to age, Glasgow coma score, outcome, intracranial pressure, and time after injury. *J Neurol Neurosurg Psychiatry* 58:145-152.
226. Shi B, Narayanan TK, Yang ZY, Christian BT, Mukherjee J (1999) Radiosynthesis and in vitro evaluation of 2-(N-alkyl-N-1'-11C-propyl)amino-5-hydroxytetralin analogs as high affinity agonists for dopamine D-2 receptors. *Nucl Med Biol* 26:725-735.
227. Sihver W, Fasth KJ, Horti AG, Koren AO, Bergström M, Lu L, Hagberg G, Lundqvist H, Dannals RF, London ED, Nordberg A, Långström B (1999) Synthesis and characterization of binding of 5-[^{76}Br]bromo-3-[[2(S)-azetidinyl]methoxy]pyridine, a novel nicotinic acetylcholine receptor ligand, in rat brain. *J Neurochem* 73:1264-1272.
228. Sihver W, Fast KJ, Ögren M, Bivehed H, Bergström M, Nordberg A, Watanabe Y, Långström B (1998) In vitro evaluation of ^{11}C-labeled (S)-nicotine, (S)-3-methyl-5-(1-methyl-2-pyrrolidinyl)isoxazole, and (R,S)-1-methyl-2-(3-pyridyl)azetidine as nicotinic receptor ligands for positron emission tomography studies. *J Neurochem* 71:1750-1760.
229. Smith DH, Okiyama K, Thomas MJ, Claussen B, McIntosh TK (1991) Evaluation of memory dysfunction following experimental brain injury using the Morris water maze. *J Neurotrauma* 8:259-269.
230. Smith DH, Okiyama K, Gennarelli TA, McIntosh TK (1993) Magnesium and ketamine attenuate cognitive

dysfunction following experimental brain injury. *Neurosci Lett* 157:211-214.
231. Smith DH, Okiyama K, Thomas MJ, McIntosh TK (1993) Effects of the excitatory amino acid receptor antagonists kynurenate and indole-2-carboxylic acid on behavioral and neurochemical outcome following experimental brain injury. *J Neurosci* 13:5383-5392.
232. Smith PK, Krohn RI, Hermanson GT, Mallia AK, Gartner FH, Provenzano MD, Fujimoto EK, Goeke NM, Olson BJ, Klenk DC (1985) measurement of protein using bicinchoninic acid. *Anal Biochem* 150: 76-85.
233. Sokoloff L, Reivich M, Kennedy C, Des Rosiers MH, Patlak CS, Pettigrew KD, Sakurada O, Shinohara M (1977) The [^{14}C]deoxyglucose method for the measurement of local cerebral glucose utilization: theory, procedure, and normal values in the conscious and anesthetized albino rat. *J Neurochem* 28:897-916.
234. Sokoloff L (1984) Modeling metabolic processes in the brain in vivo. *Ann Neurol* 15 :S1-11.
235. Sonoda M, Takano M, Miyahara J, Kato H (1983) Computed radiography utilizing scanning laser stimulated luminescence. *Radiology* 148:833-838.
236. Spence AM, Graham MM, Muzi M, Abbott GL, Krohn KA, Kapoor R, Woods SD (1990) Deoxyglucose lumped constant estimated in a transplanted rat astrocytic glioma by the hexose utilization index. *J Cereb Blood Flow Metab* 10:190-198.
237. Spence AM, Muzi M, Graham MM, O'Sullivan F, Krohn KA, Link JM, Lewellen TK, Lewellen B, Freeman SD, Berger MS, Ojemann GA (1998) Glucose metabolism in human malignant gliomas measured quantitatively with PET, 1-[C-11]glucose and FDG: analysis of the FDG lumped constant. *J Nucl Med* 39:440-448.
238. Speth RC, Johnson RW, Regan J, Reisine T, Kobayashy RM, Bresolin N, Roeske WR and Yamamura HI (1980) The benzodiazepine receptor of mammalian brain. *Federation Proceedings* 39:3032-3038.
239. Subramanyam R, Alpert NM, Hoop B Jr, Brownell GL, Taveras JM (1978) A model for regional cerebral oxygen distribution during continuous inhalation of $^{15}O_2$, $C^{15}O$, and $C^{15}O_2$. *J Nucl Med* 19:48-53.
240. Suda S, Shinohara M, Miyaoka M, Lucignani G, Kennedy C, Sokoloff L (1990) The lumped constant of the deoxyglucose method in hypoglycemia: effects of moderate hypoglycemia on local cerebral glucose utilization in the rat. *J Cereb Blood Flow Metab* 10:499-509.
241. Sullivan HG, Martinez J, Becker DP, Miller JD, Griffith R, Wist AO (1976) Fluid-percussion model of mechanical brain injury in the cat. *J Neurosurg* 45:521-534.
242. Sunami K, Nakamura T, Ozawa Y, Kubota M, Namba H, Yamaura A (1989) Hypermetabolic state following experimental head injury. *Neurosurg Rev* 12 Suppl 1:400-411.
243. Szabo L, Kovach AG, Babosa M (1983) Local effect of anaesthesia on cerebral blood flow in the rat. *Acta Physiol Hung* 62:113-121.
244. Takahashi K, Murakami M, Miura S, Iida H, Kanno I, and Uemura K (1999) Synthesis and autoradiographic localization of muscarinic cholinergic antagonist (+)N-[11C]methyl-3-piperidyl benzilate as a potent radioligand for positron emission tomography. *Appl Radiat Isot* 50: 521-525.
245. Tallman JF, Paul SM, Skolnick P, Gallager DW (1984) Receptors for the age of anxiety: pharmacology of the benzodiazepines. *Science* 207, 274-281.
246. Tanaka H, Katayama Y, Kawamata T, Tsubokawa T (1994) Excitatory amino acid release from contused brain tissue into surrounding brain areas. *Acta Neurochir Suppl (Wien)* 60:524-527.
247. Tang C, Biemond I and Lamers CBHW (1995) Localisation and quantification of cholecystocinin receptors in rat brain with storage phosphor autoradiography. *BioTechniques* 18:886-889.
248. Tanno H, Nockels RP, Pitts LH, Noble LJ (1992) Breakdown of the blood-brain barrier after fluid percussive brain injury in the rat. Part 1: Distribution and time course of protein extravasation. *J Neurotrauma* 9:21-32.
249. Teasdale G, Jennett B (1974) Assessment of coma and impaired consciousness. A practical scale. *Lancet* 2(7872):81-84.
250. Thompson MF, Bachelard HS (1977) Differences in catalytic properties between cerebral cytoplasmic and mitochondrial hexokinases. *Biochem J* 161:593-598.
251. Toulmond S, Serrano A, Benavides J, Scatton B (1993) Prevention by eliprodil (SL 82.0715) of traumatic brain damage in the rat. Existence of a large (18 h) therapeutic window. *Brain Res* 620:32-41.
252. Vink R, Yum SW, Lemke M, Demediuk P, Faden AI (1989) Traumatic spinal cord injury in rabbits decreases intracellular free magnesium concentration as measured by 31P MRS. *Brain Res* 490:144-147.
253. Vink R, Golding EM, Headrick JP (1994) Bioenergetic analysis of oxidative metabolism following traumatic brain injury in rats. *J Neurotrauma* 11:265-274.
254. Wallace MC, Teasdale GM, McCulloch J (1992) Autoradiographic analysis of ^{3}H-MK-801 (dizocilpine) in vivo uptake and in vitro binding after focal cerebral ischemia in the rat. *J Neurosurg* 76:127-133.
255. Kalsbeek WD, McLaurin RL, Harris BS 3d, Miller JD (1980) The National Head and Spinal Cord Injury Survey: major findings. *J Neurosurg* Suppl:S19-31.
256. Wei EP, Dietrich WD, Povlishock JT, Navari RM, Kontos HA (1980) Functional, morphological, and metabolic abnormalities of the cerebral microcirculation after concussive brain injury in cats. *Circ Res* 46:37-47.
257. Whiting BR, Owen JF, Rubin BH (1988) Storage phosphor X-ray diffraction detectors. *Nucl Instr Meth in Phys Res* A266, 628-635.

258. Wong EHF, Kemp JA, Priestley T, Knight AR, Woodruff GN, Iversen LL (1986) The anticonvulsant MK-801 is a potent *N*-methyl-D-aspartate antagonist. *Proc Natl Acad Sci USA* 83: 7104-7108.
259. Wong EHF, Knight AR, Ransom R (1987) Glycine modulates [^{3}H]MK801 binding to the NMDA receptor in rat brain. *Eur J Pharmacol* 142: 487-488.
260. Wong EHF, Knight AR, Woodruff GN (1988) [^{3}H]MK-801 labels a site on the N-methyl-D-aspartate receptor channel complex in rat brain membranes. *J Neurochem* 50:274-281.
261. Woodruff GN, Foster AC, Gill R, Kemp JA, Wong EH, Iversen LL (1987) The interaction between MK-801 and receptors for N-methyl-D-aspartate: functional consequences. *Neuropharmacology* 26:903-909.
262. Worley G, Hoffman JM, Paine SS, Kalman SL, Claerhout SJ, Boyko OB, Kandt RS, Santos CC, Hanson MW, Oakes WJ, Coleman RE (1995) 18-Fluorodeoxyglucose positron emission tomography in children and adolescents with traumatic brain injury. *Dev Med Child Neurol* 37:213-220.
263. Yamakami I, McIntosh TK (1989) Effects of traumatic brain injury on regional cerebral blood flow in rats as measured with radiolabeled microspheres. *J Cereb Blood Flow Metab* 9:117-124.
264. Yamakami I, McIntosh TK (1991) Alterations in regional cerebral blood flow following brain injury in the rat. *J Cereb Blood Flow Metab* 11:655-660.
265. Yamaki T, Imahori Y, Ohmori Y, Yoshino E, Hohri T, Ebisu T, Ueda S (1996) Cerebral hemodynamics and metabolism of severe diffuse brain injury measured by PET. *J Nucl Med* 37:1166-1170.
266. Yeh GC, Bonhaus DW, McNamara JO (1990) Evidence that zinc inhibits N-methyl-D-aspartate receptor-gated ion channel activation by noncompetitive antagonism of glycine binding. *Mol Pharmacol* 38:14-19.
267. Yoshida S, Murata T, Omata N, Waki A, Fujibayashi Y, Isaki K, Oka H, Yonekura Y (1998) The effect of neuronal perturbation on the uptake of [^{18}F]2-fluoro-2-deoxy-D-glucose in brain slices of the rat. *Neurosci Res* 30:271-278.
268. Yoshino A, Hovda DA, Kawamata T, Katayama Y, Becker DP (1991) Dynamic changes in local cerebral glucose utilization following cerebral conclusion in rats: evidence of a hyper- and subsequent hypometabolic state. *Brain Res* 561:106-119.
269. Zauner A, Bullock R (1995) The role of excitatory amino acids in severe brain trauma: opportunities for therapy: a review. *J Neurotrauma* 12:547-554.
270. Zeller K, Rahner-Welsch S, Kuschinsky W (1997) Distribution of Glut1 glucose transporters in different brain structures compared to glucose utilization and capillary density of adult rat brains. *J Cereb Blood Flow Metab* 17:204-209.
271. Zubieta JK, Koeppe RA, Mulholland GK, Kuhl DE, Frey KA (1998) Quantification of muscarinic cholinergic receptors with [^{11}C]NMPB and positron emission tomography: method development and differentiation of tracer delivery from receptor binding. *J Cereb Blood Flow Metab* 18:619-631.